

DOT/FAA/AR-96/95

Office of Aviation Research
Washington, D.C. 20591

The Potential for Fuel Tank Fire and Hydrodynamic Ram From Uncontained Aircraft Engine Debris

January 1997

Final Report

This document is available to the U.S. public
through the National Technical Information
Service, Springfield, Virginia 22161.



U.S. Department of Transportation
Federal Aviation Administration

NOTICE

This document is disseminated under the sponsorship of the U.S. Department of Transportation in the interest of information exchange. The United States Government assumes no liability for the contents or use thereof. The United States Government does not endorse products or manufacturers. Trade or manufacturer's names appear herein solely because they are considered essential to the objective of this report.

This report reflects BlazeTech Corporation's best judgment in light of the information available to it at the time of preparation. Any use of this report or any reliance on or decision to be made based on it by any party (including third party, if any) is the responsibility of such party. BlazeTech Corporation accepts no responsibility for damages, if any, suffered by any party as a result of decisions made or actions taken based on this report.

1. Report No. DOT/FAA/AR-96/95		2. Government Accession No.		3. Recipient's Catalog No.	
4. Title and Subtitle THE POTENTIAL FOR FUEL TANK FIRE AND HYDRODYNAMIC RAM FROM UNCONTAINED AIRCRAFT ENGINE DEBRIS				5. Report Date January 1997	
				6. Performing Organization Code	
7. Author(s) N.A. Moussa, M.D. Whale, D.E. Groszmann, and X.J. Zhang				8. Performing Organization Report No.	
9. Performing Organization Name and Address BlazeTech Corporation 21 Erie Street Cambridge, MA 02139-4260				10. Work Unit No. (TRAIS)	
				11. Contract or Grant No.	
12. Sponsoring Agency Name and Address U.S. Department of Transportation Federal Aviation Administration Office of Aviation Research Washington, DC 20591				13. Type of Report and Period Covered Final Report	
				14. Sponsoring Agency Code AAR-431	
15. Supplementary Notes FAA William J. Hughes Technical Center COTR: Mr. John Reinhardt and Mr. Robert Pursel .					
16. Abstract This report addresses the potential consequences of the impact and penetration of fuel tanks by debris from uncontained engine failures on commercial jet aircraft. The report presents a brief review of accident data and of the pertinent technical literature, a detailed analysis of in-tank ignition by hot fragments, and parametric calculations using a computer code for hydrodynamic ram. the results suggest that in-tank fire and hydrodynamic ram can be produced by engine debris, though their expected probability of occurrence is very low.					
17. Key Words In-tank fire, Hot fragment ignition, Hydrodynamic ram, Uncontained engine failures, Jet engines, Probability, Aircraft, Explosion			18. Distribution Statement This document is available to the public through the National Technical Information Service (NTIS), Springfield, Virginia 22161.		
19. Security Classif. (of this report) Unclassified		20. Security Classif. (of this page) Unclassified		21. No. of Pages 80	
				22. Price	

TABLE OF CONTENTS

	Page
EXECUTIVE SUMMARY	xi
1. INTRODUCTION	1
1.1 Background	1
1.2 Scope and Approach	1
2. REVIEW OF UNCONTAINED ENGINE FAILURES	2
2.1 Sources of Data	2
2.2 Frequency of Uncontained Engine Failures	2
2.3 Sequence of Events After Uncontained Failure	3
2.3.1 Fuel Tank Penetration	6
2.3.2 In-Tank Fire or Explosion	6
2.3.3 Hydrodynamic Ram	8
2.3.4 Probability Estimates for the Overall Hazard	8
2.4 Other Hazards From Uncontained Engine Failure	10
3. LITERATURE REVIEW ON IMPACT-INDUCED FIRE AND EXPLOSION INSIDE FUEL TANKS	10
3.1 Fuel Tank Ullage Flammability	12
3.1.1 Flammability Envelopes Under Static (Equilibrium) Conditions	12
3.1.2 Flammability Envelopes Under Dynamic Conditions	12
3.2 Ignition and Overpressure in Gunfire Impact Tests	15
3.3 Risk Assessment of Ignition for the Concorde	17
4. POTENTIAL FUEL TANK IGNITION BY ENGINE DEBRIS	20
4.1 Temperature-Time Requirements for Ignition	21
4.2 Fragment Motion	22
4.3 Fragment Entering Ullage	23
4.3.1 Heat Transfer	23
4.3.2 Film Temperature-Time History Versus Ignition Requirements	26
4.3.3 Fuel/Air Mixture	28
4.4 Fragment Entering Liquid Fuel	30

4.4.1	Heat Transfer From Fragment	30
4.4.2	Temperature Profile	31
4.4.3	Film Temperature-Time History Versus Ignition Requirements	32
4.4.4	Fuel/Air Mixture	33
4.4.5	Bubble Rise	35
4.5	Passage from Liquid Fuel to Ullage	38
4.6	Analysis Limitations	39
4.7	Comparison of Present Study with Wallin	39
5.	HYDRODYNAMIC RAM CALCULATIONS	41
5.1	Brief Description of ERAM	41
5.2	Distribution of Typical Fragment Characteristics	41
5.2.1	Blade Fragment Models	42
5.2.2	Disk Sector Fragment Models	43
5.3	Description of a Typical Fuel Cell	44
5.4	ERAM Data Input	44
5.5	Results of Calculation	44
6.	POSSIBLE MITIGATION MEASURES	47
6.1	Mitigation of Fire and Explosion	47
6.1.1	Ullage Inerting	47
6.1.2	Foams	48
6.1.3	Extinguishing Agents	48
6.2	Mitigation of Hydrodynamic Ram	48
7.	SUMMARY AND CONCLUSIONS	49
7.1	Summary	49
7.1.1	In-Tank Fuel Ignition by Engine Debris	50
7.1.2	Hydrodynamic Ram by Engine Debris	52
7.2	Conclusions	53
8.	REFERENCES	54

APPENDICES

A—Description of Key Accidents

B—Asperity from Fragment Impact: Its Detachment and High Temperature Formation

LIST OF FIGURES

Figure	Page
1 Fault Tree for Uncontained Engine Failure – Rotating Components	4
2 Fault Tree for Uncontained Engine Failure – Flight Modes	5
3 Pressure Altitude – Temperature Limits of Flammability for Jet-A and Jet-B Type Fuels in Air Under Equilibrium (or Static) Conditions (Kuchta, 1985)	14
4 Flammability Limits Including Effects of Air Release and Tank Dynamics (CRC Report No. 530, 1983)	16
5 Combustion Overpressure as a Function of Fuel Initial Temperature for Gunfire Tests for JP-5 and -8 (90-Gallon Tank, 4-Inch Fuel Depth at Atmospheric Pressure)	18
6 Two Scenarios of Fragment Entering Fuel Tank	20
7 Velocity and Distance of Typical Inconel Fragment Traveling Through Ullage; Initial $Re_D = 6.8 \times 10^4$	24
8 Velocity and Distance of Typical Inconel Fragment Traveling Through Liquid Fuel; Initial $Re_D = 1.4 \times 10^6$	24
9 Temperature–Time History of Film Around Fragment and Temperature–Time Required for Ignition in Ullage at Sea Level ($V_o = 237$ m/s, 59 g Fragment)	27
10 Film Temperature–Time History and Temperature–Time Required for Ignition in Ullage at an Altitude of 10,000 m ($V_o = 237$ m/s, 59 g Inconel Fragment)	27
11 Temperature Profile of Inconel Fragment Traveling Through Liquid Kerosene	32
12 Temperature–Time History of Vapor at Boiling Surface and Temperature–Time Required for Ignition in Liquid Fuel	33
13 Mass Fractions of Vapor in the Wake of a Fragment in Liquid Fuel	35
14 Diameter of a Bubble Rising Through Liquid Fuel to the Free-Surface of the Fuel	37
15 Temperature of a Bubble Rising Through Liquid Fuel to the Free Surface	38
16 Peak Wall Pressure Evolution After Fragment Impacts the Fuel Tank	45

17	Peak Stress in the Tank Wall as a Function of Time	46
18	Critical Initial Hole Diameter on the Wall (Maximum Allowable Initial Hole Size as a Function of Time). The Two Horizontal Lines Represent the Initial Hole Size Due to the Perforation of Blade and Disk Fragments.	46

LIST OF TABLES

Table		Page
1	Description of Pertinent Accidents Involving Puncture of the Fuel Tank	7
2	Summary of Uncontained Turbine Engine Rotor Events From the FAA/SAE Report (1994)	9
3	Pertinent Accidents Resulting in Severed Fuel Lines	11
4	Summary of Key Studies on Flammability of Aircraft Tank Ullage Systems	13
5	The Ignition Risk Factors From Wallin (1976)	19
6	Properties of Jet-A Fuel	25
7	Properties of Disk Fragment Materials From Incropera and DeWitt (1985)	25
8	Effect of Tank Dynamics on Flammability Limits	30
9	Comparison of Ignition Risk Factors From Wallin (1976) With Present Study	40
10	Typical Characteristics of Fragments From Blades and 120 Degree Disk Segments for Commercial Aircraft Engines	42

NOMENCLATURE

A_f	=	area of the fragment perpendicular to the flow
Bi	=	Biot number
Bo	=	Bond number
c	=	specific heat of fragment
C_D	=	drag coefficient
$c_{v,b}$	=	heat capacity at constant volume for the gas within the bubble of mass m_b
D	=	diameter
E	=	activation energy
E_R	=	probability of an explosion
F	=	probability of the ignition of a fire
F_D	=	drag force
Fo	=	Fourier number
f	=	pre-exponential factor
g	=	gravitational acceleration
H_R	=	probability of fire becoming catastrophic
h	=	heat transfer coefficient
h_{fg}	=	heat of vaporization
I_R	=	ignition probability
k	=	thermal conductivity
k_v	=	thermal conductivity of vapor
L	=	length
L_R	=	probability of not landing safely with a catastrophic fire
Mo	=	Morton number
m	=	mass
m_e	=	mass of air entrained
M_v	=	fuel molecular weight
N	=	number of drops intercepted by fragment
n	=	order of the reaction
p	=	pressure
Pr	=	Prandtl number
P_v	=	pressure of the vaporized fuel within the bubble
p_{drops}	=	effective vapor pressure of fuel drops suspended in ullage
p_v	=	fuel vapor pressure
q''	=	flux of energy
R	=	probability of hydrodynamic ram
Re	=	Reynolds number
Re_D	=	Reynolds number based on length = D
\mathfrak{R}	=	universal gas constant
s	=	drop density
T	=	absolute temperature
T_R	=	proportion of flight phase that fuel is present in the penetrated tank
T_S	=	surface temperature of the fragment at the point of boiling
T_v	=	temperature of the vaporized fuel within the bubble

t_c	=	ignition delay time
U	=	probability of an uncontained engine failure
V	=	velocity
Vol_{air}	=	volume of entrained air
W	=	watts
x	=	fragment travel distance
ε	=	void fraction
ϵ	=	emissivity
ν	=	kinematic viscosity
μ	=	viscosity
ρ	=	fluid density
σ	=	surface tension
σ_p	=	stress in plate
τ	=	daytime constant
χ	=	fuel mole fraction

Subscripts

l	=	liquid
v	=	vapor
vap	=	vapor
o	=	reference state
∞	=	free stream

Abbreviations

AAIB	=	Aircraft Accident Investigative Board
AIR	=	Aircraft Incident Report
CAA	=	Civil Aviation Administration
CCOC	=	Combustion Chamber Outer Case
DOT	=	Department of Transportation
ERAM	=	Computer Code on Hydrodynamic Ram
FAA	=	Federal Aviation Administration
FMEA	=	Failure Mode and Effect Analysis
FTA	=	Fault Tree Analysis
HPT	=	High Pressure Turbine
LP	=	Low Pressure
NIBB	=	Nitrogen Inerted Bladder by Boeing
NTSB	=	National Transportation Safety Board
OBIGGS	=	On Board Inert Gas Generator
R&D	=	Research and Development
SAE	=	Society of Automotive Engineers
SST	=	Supersonic Transport

EXECUTIVE SUMMARY

Uncontained engine failures in commercial aircraft produce high-speed, hot fragments that can impact and penetrate fuel tanks. This report addresses two events that can be potentially produced by such an impact. They are ignition of the fuel vapors when a hot fragment enters the ullage (space above the liquid fuel level in the tank) and hydrodynamic ram when a fragment enters the liquid fuel with sufficient kinetic energy. Either of these events can produce overpressure inside the tank with a potential for tank rupture and an immediate loss of the aircraft.

Prior to this project, the possibility of a fire inside a fuel tank was mostly discounted because the fuel temperature under normal operating conditions is below the flash point of Jet-A fuel, i.e., the ullage composition is outside the static flammability envelope of Jet-A fuel. Furthermore, hydrodynamic ram was not recognized as a potential hazard in commercial aircraft, as evidenced by the lack of its study in the open literature (except for military aircraft under combat conditions).

This report presents an exploratory assessment of these two hazards. It covers a brief review of accident data, a review of the pertinent literature on military aircraft where these events have long been recognized, an analysis of ignition by hot fragments, and use of an existing computer code on hydrodynamic ram. The analytical and computer calculations adapted the military data to commercial aircraft conditions. The results suggest that these events can happen, although with a very low probability. A summary of evidence for these two events follows.

First, tests in the literature show that dynamic processes can broaden significantly the ullage flammability envelope for Jet-A over the static case. A mist of fuel droplets can be formed inside the tank due to fuel sloshing because of aircraft motion and vibration in normal flight and fragment motion through the fuel after tank penetration. When these droplets are vaporized by a hot fragment, the fuel vapor pressure is raised locally, thus making the ullage flammable and increasing the possibility of ignition inside the tank.

Second, the risk of fire and explosion in aircraft fuel tanks in the Concorde SST due to uncontained failure of the Olympus 593 engine was initially recognized in a British Aerospace report by Wallin (1976). The probability of ignition for Jet-A was estimated, based on judgment, to vary from 0.05 to 0.8 depending on fragment trajectory and fuel temperature (starting at -50°C, well below the flash point). In a postscript to this report, the risk of ignition was dismissed because no such event had been observed in 21 historical cases of uncontained engine failure.

Third, we conducted an analysis of fuel ignition by a moving hot fragment. The analysis accounts for heat transfer from the fragment to a surrounding fuel vapor film as a function of time. We compared the film temperature-time history to that required for fuel ignition as measured in fundamental studies. This comparison delineated the conditions of fuel ignition and quenching and their dependence on fuel properties and fragment size, temperature, and velocity. For typical conditions with Jet-A and a blade fragment from the turbine section impacting the ullage, we predict ignition for a blade temperature exceeding about 1000° K, which is above the operating temperature of titanium but well below that of Inconel blades. Also, the predicted threshold temperature for ignition increases with altitude. For the same conditions, but with a

fragment impacting the liquid fuel, we predict quenching. All of these predictions appear plausible.

Fourth, we used an existing computer code for hydrodynamic ram (ERAM) to assess the potential damage to a fuel tank. This code is considered to be the state of the art, though it contains many simplifications and approximations that can be improved. It accounts for the forces acting on the fragment, the transfer of energy to the fluid, the pressure rise, the resulting stress and strain in the tank walls, and a fracture criteria for wall failure. Parametric calculations were performed for a typical fan blade and a 120 degree LP turbine disk segment (potential fragments with the largest kinetic energy) at typical velocities impacting an aluminum tank. For these two fragments, six cases were considered to model various orientations of the fragments along their trajectories. In all cases except one, tank wall failure is predicted, even when allowing for a wide margin of error. These results suggest that hydrodynamic ram can rupture the tank, causing large amounts of fuel to exit the tank and accentuating the fire hazard. Loss of fuel may also lead to some loss of center of gravity control. Thus the hydrodynamic ram hazard should not be dismissed.

Our review of historical aircraft accidents involving fragments from uncontained engine failures was limited in scope, and some of the identified accident reports could not be obtained. Nevertheless, we did find several reports of fragments penetrating fuel tanks with significant damage to the tank, accompanied by loss of fuel. There were two reports of in-tank fires which also produced explosions. Detailed examination of these accidents shows that the tank ullage vapor can ignite, although not necessarily due to fragment penetration. Hydrodynamic ram was not mentioned. Also, the data show that fuel tank penetrations produce scenarios outside the scope of this project; for example, fuel leakage into dry bays and engine nacelles and the potential for fire therein and fuel leakage outside the aircraft and either its ingestion by an engine or its puddling on the ground producing a pool fire.

In summary, our study indicates that fragment-initiated in-tank fire and hydrodynamic ram did not occur in the past but can occur, though the conditions required for their occurrence have a very low probability. To estimate a rough order of magnitude for this probability, we used historical data from various sources. The data suggest that the failure probability of an uncontained engine on commercial aircraft is on the order of 4.4×10^{-7} events/engine hour. Since fragment-induced in-tank fire and hydrodynamic ram have not been reported as yet in any of the 621 uncontained engine failures in the period 1962-1989, an upper bound on such an occurrence would be 1 in 622 (i.e., assuming it were the next accident to occur), or about 0.0016. The corresponding **upper bound** on the overall probability of these two events is thus on the order of 7×10^{-10} events/engine hour, a very low number.

Finally, protection methods for military aircraft, particularly for in-tank fires, are reviewed. These systems incur weight, volume, and/or auxiliary power penalties and require the addition of complex systems with their own reliability and maintenance issues. Their suitability to commercial aircraft would require cost benefit analyses.

1. INTRODUCTION.

1.1 BACKGROUND.

Uncontained engine failure can produce high-speed fragments varying in weight from the order of grains to pounds. These fragments may impact and damage surrounding structures and equipment. Of particular concern are impacts to fuel tanks and the potential for either fire or hydrodynamic ram inside the fuel tank. Either of these two events can produce overpressure inside the tank, tank rupture, fuel release from the tank, loss of center of gravity control, secondary fires, and aircraft loss. Accordingly, the Federal Aviation Administration (FAA) initiated an investigation of these two hazard mechanisms.

Before this study, the possibility of a fire inside the fuel tank has been mostly discounted by industry because the fuel temperature under normal operating conditions is below the flash point of Jet-A, i.e., the fuel/air mixture inside the tank is below the flammable range. Furthermore, hydrodynamic ram has not been studied as a potential hazard in commercial aircraft, while it has been studied in military aircraft under combat conditions.

Accordingly, the objective of this study was to investigate the potential for fragment-initiated fire and hydrodynamic ram inside a fuel tank on commercial aircraft to determine whether such events can be caused by uncontained engine failures.

1.2 SCOPE AND APPROACH.

The scope of this study covers commercial airliners with turbine engines using Jet-A fuel. General aviation and rotorcraft are excluded. It is assumed that an uncontained engine failure has occurred and that some fragments have impacted the fuel tank with a sufficiently large kinetic energy to puncture and penetrate the tank. Impacts against fuel and hydraulic lines are excluded. Under these conditions, the study focuses on subsequent events; namely, fire and hydrodynamic ram. These sequences of events have low and unknown probabilities of occurrence. Still, they are examined because the potential consequence may be a catastrophic loss of the aircraft.

The approach used relies principally on a study of the fundamental processes involved in these two mechanisms to establish what can happen and what are the governing parameters. This was supported by information obtained from the literature on military aircraft, including test data on fire and explosion, and a computer model of hydrodynamic ram. This information was adapted to commercial aircraft conditions as much as possible using typical fragment sizes, velocities, and temperatures and the properties of Jet-A. The analysis was also supplemented by a brief review of historical aircraft accidents to place the above scenarios in the perspective of actual events.

Section 2 presents a preliminary review of historical accidents involving uncontained engine failures. The focus was to characterize the sequence of events triggered by uncontained engine debris that impacts a fuel tank. Section 3 presents pertinent information from the literature on the flammability of the vapor space (ullage) inside an aircraft fuel tank, and on in-tank fires and explosions under gun fire test conditions. Section 4 presents a theoretical analysis of ignition inside a fuel tank by typical debris penetrating the tank. The focus is on a blade from the high-

pressure turbine (highest initial blade temperature) impacting the fuel tank above and below the liquid level. Section 5 applies an existing computer code on hydrodynamic ram to a typical fuel tank impacted by high-energy fragments, namely a fan blade or a 120 degree segment of a low-pressure turbine disk. Section 6 summarizes briefly the mitigation methods used by the military aircraft to protect fuel tanks against fire and hydrodynamic ram. Section 7 presents a summary of the major findings in this report and the key conclusions. Supporting information and analyses are presented in appendices A and B.

2. REVIEW OF UNCONTAINED ENGINE FAILURES.

This section presents a brief review of aircraft accident data on uncontained engine failures. The literature contains much information on the causes of uncontained engine failures but not on the sequence of events following the failure. In-tank fires or hydrodynamic ram caused by fragments from uncontained engine failures were not reported. However, in-tank fires and explosions caused by other means have been observed, although very rarely.

The scenarios of interest in this study cover a sequence of key events that may lead to catastrophic aircraft loss. These events include uncontained engine failure, penetration of the fuel tank, ignition of the fuel inside the tank or hydrodynamic ram, pressure rise inside the tank, and tank rupture. Many of these events have been reported as occurring either alone or in various combinations, but not in this precise sequence. The main findings from the data review are presented below. Detailed information on selected accidents is presented in appendix A.

2.1 SOURCES OF DATA.

Data from previous accidents involving uncontained engine failures were compiled from many sources including the National Transportation Safety Board (NTSB) accident reports, NTSB special reports, the Air Accidents Investigation Branch, computerized databases, and three Society of Automotive Engineers (SAE) reports. We concentrated on accidents involving large commercial aircraft documented in Title 14 CFR Part 121 of the NTSB Annual Review of Aircraft Accident Data. Part 121 focuses on the certification and operations of domestic, flag, and supplemental air carriers and commercial operators of large aircraft. Once the accidents of interest were identified, the individual aircraft accident reports from the NTSB were obtained and reviewed. Some of the requested reports were not available from the NTSB. We also used a number of other sources of accident data which are outlined in appendix A, including the locations of the sources and the relevant dates.

2.2 FREQUENCY OF UNCONTAINED ENGINE FAILURES.

The most comprehensive compilations of accidents on uncontained engine failure are the three SAE Aircraft Incident Report (AIR) reports on aircraft engine containment. SAE AIR 1537 (1977) covers the years 1962-1975, SAE AIR 4003 (1987) covers the years 1976-1983, and SAE AIR 4770 (1994) covers the years 1984-1989. These reports focused on the location of the failure (fan, compressor, etc.), the flight stage at failure (takeoff, climb, etc.), and when determinable, the cause of the failure (fatigue, material defect, etc.).

The SAE AIR reports provide enough data to estimate the probability of failure of uncontained engines using fault tree analysis (FTA). FTA is a standard method to relate the failure probability of a system to that of its constitutive elements. These elements could be components or subsystems depending on the desired level of details and the available data. The method describes the interactions between the elements in graphical form using logical decisions or gates (AND and OR). Thus, Boolean algebra can be used to combine the failure rates of the elements to estimate that of the overall system. An alternate method is failure modes and effect analyses, FMEA. However, FTA was more suitable in this project.

The data in SAE AIR 4770, the most recent report, are presented in this section as fault trees in figures 1 and 2. All failure probability numbers in these figures are based solely on the historical data in the SAE report. The top event in both trees is the uncontained engine failure with a probability (U) of about 4.4×10^{-7} events/engine hour. The second level in both trees consists of three engine stages: fan, compressor, and turbine. Elements with insignificant failure rates are not shown in these figures.

The second level in figure 1 shows that the most frequent cause of uncontained engine failure was a turbine part failure with 2.1×10^{-7} events/engine hour. Compressor part failures were the least frequent cause (3.7×10^{-8} events/engine) and may be due to the heavy shielding used for the high pressures. The third level in figure 1 shows subsystems to each of the three engine stages: blade, disk, or spacer. Blade failures are more frequent than the failure of the other subsystems parts.

The third level in figure 2 shows the nine different flight modes: takeoff, climb, cruise, descent, landing, reverse, approach, ground run, or unknown. Takeoff is the flight mode with the highest probability of failure for all three engine stages: fan, compressor, and turbine. During takeoff, the fan part failure has the highest probability among the three stages (1.2×10^{-7} events/engine hour).

2.3 SEQUENCE OF EVENTS AFTER UNCONTAINED FAILURE.

There was no compilation of event sequences after uncontained engine failure in the open literature comparable to the SAE AIR reports. Clearly, such sequences are very case specific and difficult to establish. They were analyzed and documented by accident investigators only for the most important historical accidents.

The two scenarios of interest in this study are fire and hydrodynamic ram in fuel tanks initiated by fragments from uncontained engine failures. We found no reports describing these particular scenarios in our search of commercial aircraft accidents. However, information relevant to the major events within these scenarios was found for

- fuel tank penetration,
- in-tank fire or explosion, and
- hydrodynamic ram.

Based on Historical
Accident Data from an
SAE AIR 4770 "Report on
Aircraft Engine
Containment"
(1984-1989)

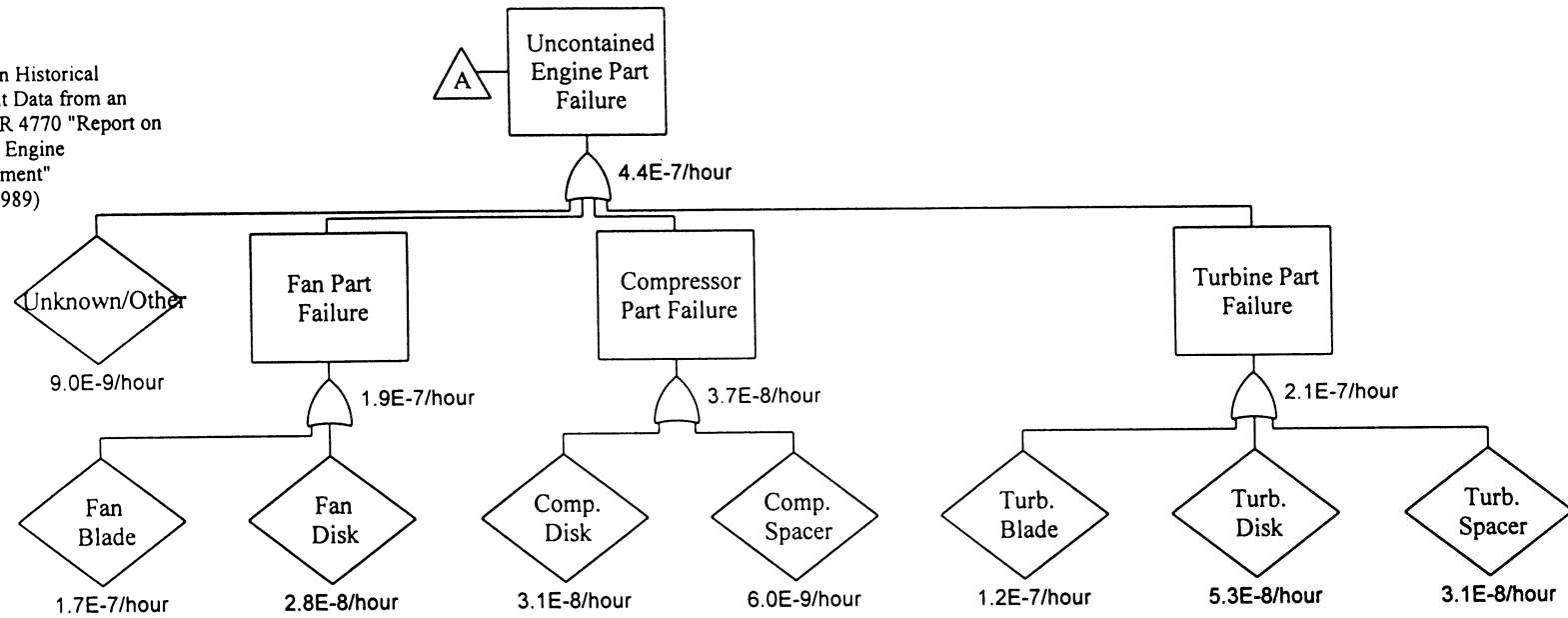


FIGURE 1. FAULT TREE FOR UNCONTAINED ENGINE FAILURE—ROTATING COMPONENTS

Based on Historical Accident Data
from an SAE AIR 4770 "Report on
Aircraft Engine Containment"
(1984-1989)

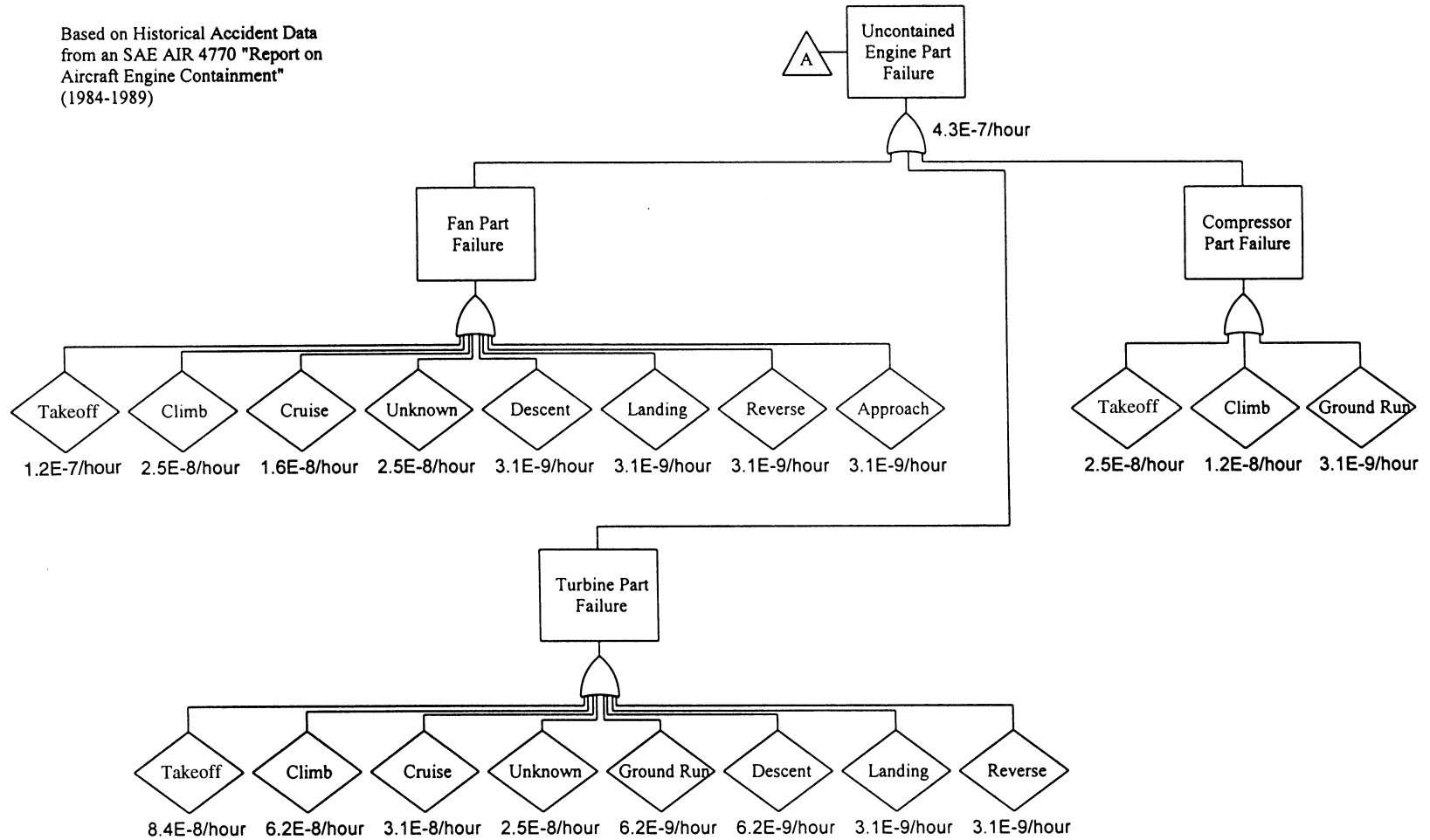


FIGURE 2. FAULT TREE FOR UNCONTAINED ENGINE FAILURE—FLIGHT MODES

2.3.1 Fuel Tank Penetration.

The data on aircraft accidents involving fuel tank puncturing by debris from uncontained engine failures are summarized in table 1. The table gives the date and location of the accident, the aircraft model, the uncontained engine event, the system damaged by the debris and a brief description of the consequence. The table illustrates that engine fragments do escape the engine and its nacelle and penetrate fuel tanks.

Statistical data for fuel tank penetration after engine failure were reported by the NTSB Special Study of Turbine Engine Rotor Disk Failures (1974). The study covered 41 cases of engine disk failures in public transport aircraft from 1962 to 1973; over 15 percent of these cases had fuel tank penetration and subsequent fuel leakage. There was no mention of a fuel tank penetration without a leak. We assume that 15 percent of uncontained engine failures lead to fuel tank penetration, with or without subsequent leaks. This can be expressed as a probability ($P = 0.15$) for the uncontained debris to reach and penetrate the tank.

The NTSB data are limited and older than those of the SAE AIR report used in section 2.2, but were used since no newer study was available. Using the probability of uncontained engine failure (U) from section 2.2, the probability of fuel tank penetration by a fragment from an engine failure is of the order

$$\begin{aligned} U \times P_p &= 4.4 \times 10^{-7} \text{ uncontained engine failure / engine hour} \\ &\times 0.15 \text{ tank penetration / uncontained engine failure} \\ &= 6.6 \times 10^{-8} \text{ tank penetration / engine hour} \end{aligned}$$

2.3.2 In-Tank Fire or Explosion.

Of the accident data presented in table 1, two cases involved fires within the tanks, which were also suspected of being low-order (i.e., subsonic) explosions. We were able to obtain detailed accident reports on these two cases which are summarized below with more detail given in appendix A.

The first case is the August 22, 1985, accident in Manchester, UK. A Boeing 737 with Pratt and Whitney JT-8D engines suffered an uncontained failure of the left engine, initiated by a failure of the No. 9 combustion can, which had been repaired. The forward section of the No. 9 combustion can was ejected through the left engine combustion casing which was split open, causing substantial secondary damage to the engine and nacelle. A fuel tank access panel on the lower surface of the left wing immediately outboard of the engine was punctured, producing a large hole in the base of the main fuel tank. According to the accident report, the left engine nacelle and adjacent wing areas were damaged by fire and the wing suffered additional damage caused by an explosive overpressure within the fuel tank when the fuel vapor in the tank was ignited by some unexplained means.

TABLE 1. DESCRIPTION OF PERTINENT ACCIDENTS INVOLVING PUNCTURE OF THE FUEL TANK

Date	Location	A/C Model	Event	Damage	Result
1/19/95	Brazzaville, Congo	B747	<ul style="list-style-type: none"> first-stage disk of high-pressure turbine ruptured during flight 	<ul style="list-style-type: none"> debris punctured fuel tank 	
8/22/85	Manchester, England	B737-236	<ul style="list-style-type: none"> uncontained failure of the left engine, initiated by a failure of the No. 9 combustor 	<ul style="list-style-type: none"> combustor can struck and fractured an under-wing fuel tank access panel 	<ul style="list-style-type: none"> fire ignited and was directed into the fuselage by engine reverse buckets fuel tank experienced a rapid over-pressure due to ignition of the fuel vapor in the tank
8/30/84	Douala, Cameroon	B737-200	<ul style="list-style-type: none"> right engine failed and fragments of disc no. 7 from high-pressure compressor escaped the engine 	<ul style="list-style-type: none"> debris impacted right wing between the fuselage and engine, perforating the wing tank 	<ul style="list-style-type: none"> fuel leaked onto the ground and ignited fire destroyed the aircraft
3/22/84	Calgary	B737-200	<ul style="list-style-type: none"> 13th stage compressor disk failed 	<ul style="list-style-type: none"> fragments of the disk punctured the fuel tanks 	<ul style="list-style-type: none"> fire destroyed the aircraft
3/17/82	Sanaa, N. Yemen	A300B	<ul style="list-style-type: none"> stage 1 disk of high-pressure turbine ruptured from low cycle fatigue 	<ul style="list-style-type: none"> fuel tank punctured 	<ul style="list-style-type: none"> fire destroyed aircraft
2/15/75	Hong Kong	B707	<ul style="list-style-type: none"> front portion of No. 3 engine up to the second-stage fan blades completely separated from the engine 	<ul style="list-style-type: none"> debris from No. 3 engine entered No. 4 engine causing damage to fan blades and puncturing the wing tank at two places 	<ul style="list-style-type: none"> severe fuel leak from the wing tank when the aircraft landed no fire occurred
11/3/73	Albuquerque, NM	DC10-10	<ul style="list-style-type: none"> first-stage fan of the No. 3 (wing-mounted) engine disintegrated 	<ul style="list-style-type: none"> debris penetrated fuel tank, entered into the other engines, and blew out a window 	<ul style="list-style-type: none"> one passenger was killed after being sucked out of the window
9/18/70	San Francisco, CA	B747-121	<ul style="list-style-type: none"> No. 1 engine had an uncontained failure in the second-stage turbine disk rim turbine blades and rim fragments ejected from engine 	<ul style="list-style-type: none"> debris penetrated the HPT case, engine cowling, adjacent aircraft structure, two fuel tank access plates, and severed fuel lines 	<ul style="list-style-type: none"> intense fire
6/28/65	San Francisco, CA	B707-321B	<ul style="list-style-type: none"> No. 4 engine separated from the wing 	<ul style="list-style-type: none"> approximately 25 feet of the right outboard wing torn from the aircraft 	<ul style="list-style-type: none"> fire and puncture damage around the wing separation line on the remaining wing section explosive overpressure of reserve tank

Although the possibility is unlikely that the ignition of the fuel vapor in the tank and subsequent explosion in this accident were caused by a fragment, the fact that the ullage vapors can be ignited is an important finding.

The second case involved a low-order explosion of a fuel tank on a Boeing 707 in San Francisco, Calif., on June 28, 1965. A disk failure in the No. 4 engine resulted in an explosion that separated the engine from the wing. The lower skin separated from the aircraft, taking the attaching flanges of both spars with it. The reserve tank was damaged by the overpressure. According to the NTSB, the damage was the result of a low-order explosion. While the source of ignition could not be determined, it was attributed to either auto-ignition, burn-through, or hot-point ignition from a localized hot spot.

Thus, the data presented in table 1 and in this section indicate that uncontained engine failures may lead to (1) the penetration of the fuel tank, (2) ignition of the fuel inside the tank, and (3) tank rupture, with events (1) and (2) not necessarily related.

In-tank explosions have been reported in accidents not involving uncontained engine failures, such as the explosions of the center fuel tank in a Boeing 737 on the ground in Manila, Philippines, on 5/11/90, and in a Boeing 747 flying off the coast of Long Island, New York, on 7/17/96. The causes of these accidents have not been determined as of the writing of this report. Still, these accidents show that a fuel tank can explode, even though it is a very rare event.

2.3.3 Hydrodynamic Ram.

Hydrodynamic ram refers to the overpressure produced by the motion of a fragment inside a fuel tank. Hydrodynamic ram was not mentioned in any of the accident data that were reviewed. However, there are numerous reports on damage to the fuel tanks and, occasionally, reports on fuel tank ruptures and the outpouring of fuel from the tank. Tank rupture may be caused by the development of pressure forces inside the fuel tank – although one does not know whether they are due to combustion, hydrodynamic ram, or severe dynamic forces. The lack of specific reports on hydrodynamic ram is not surprising in view of the generally poor recognition of this phenomena (compared to combustion). Still, one can not conclude from the examined data whether it has never occurred or was simply never recognized.

2.3.4 Probability Estimates for the Overall Hazard.

From our brief review of historical data on commercial aircraft, we found no accident where engine fragments triggered the events of interest directly. Still, our review of test data and our theoretical analyses indicate that these events can happen as will be presented in sections 3 to 5. We can estimate the probability of in-tank fire, explosion, or hydrodynamic ram event produced by a fragment from an uncontained engine failure as

$$probability = U \times [F + E_R + R] \quad (1)$$

where U was discussed in section 2.3.1 and F is the probability of a fire, E_R is the probability of an explosion, and R is the probability that there is no ignition but that hydrodynamic ram ruptures the tank.

Now we need a probability for F , E_R , and R . Development of a quantitative estimate for F can be illustrated as follows:

- a. Estimate the distribution of fragment size, velocity, and trajectory for an uncontained engine event.
- b. For each fragment condition, determine whether the fragment reaches and penetrates a fuel tank.
- c. For each tank penetration in b, estimate whether ignition would occur based on the analysis of section 4 for a given flight condition (i.e., the fuel temperature, liquid level, and aircraft altitude).
- d. Combine the above over the range of fragment conditions and flight profiles to determine the fraction (F) that produces ignition.

Similar values can be developed for E_R and R . We use accident data to develop these values.

According to the FAA/SAE Committee on Uncontained Turbine Engine Rotor Events, there were a total of 621 uncontained rotor events between January 1962 and December 1989. (See table 2.)

TABLE 2. SUMMARY OF UNCONTAINED TURBINE ENGINE ROTOR EVENTS FROM THE FAA/SAE REPORT (1994)

Report	Period	All Categories
SAE AIR 1537	1962- 1975	275
SAE AIR 4003	1976-1983	203
SAE AIR 4770	1984-1989	<u>143</u>
TOTALS	1962-1989	621

Since the scenario of concern has not occurred in any of these 621 accidents, we can estimate an **upper bound** on the combined probability of (E_R+F+R) by assuming that it will happen as the next accident in table 2. The upper bound on the probability becomes 1 event in 622 accidents, i.e., on the order of 0.0016.

Then, our estimate of an **upper bound** on the probability of a fire, explosion or ram event produced by a fragment from an uncontained engine failure is

$$\begin{aligned} \text{probability} &= 4.4 \times 10^{-7} \text{ uncontained engine failure / engine hour} \\ &\times 0.0016 \text{ event / uncontained engine failure} \\ &= 7 \times 10^{-10} \text{ event / engine hour} \end{aligned}$$

This is merely a rough estimate based on extrapolation of existing data. There are other methods of reaching an estimate, such as a detailed risk assessment. This would require more data and detailed calculations of fire, explosions, and hydrodynamic ram within the fuel tank as outlined above.

We conclude that fuel tank fire, explosion, and hydrodynamic ram have a very low, but not impossible, chance of occurrence.

2.4 OTHER HAZARDS FROM UNCONTAINED ENGINE FAILURE.

Most of the accidents reviewed above resulted in fuel leakage from damaged fuel tanks. Uncontained engine failure has resulted in the severing of fuel and hydraulic lines as summarized in table 3. Fuel (or other flammable fluids) can leak into dry bays and engine nacelles, pour onto the ground (for a stationary aircraft), or be ingested by a nearby engine. The fires resulting from such leakage can pose a great threat to an aircraft. Such scenarios were outside the scope of this study. However, they have happened in the past (such as the Manchester and the Sioux City accidents) and should also be considered.

Since historical evidence was fragmented and limited, we gave particular attention in this project to what might happen based on considerations of the fundamental processes involved in fuel tank ignition and hydrodynamic ram.

3. LITERATURE REVIEW ON IMPACT-INDUCED FIRE AND EXPLOSION INSIDE FUEL TANKS.

This section presents pertinent information from the literature on fire and explosion hazards inside an aircraft fuel tank containing Jet-A fuel. It is well known that Jet-A has a low volatility and a flash point higher than ambient temperature. Thus, the fuel vapor/air concentration inside a vented aircraft tank at typical ambient temperatures is not flammable at sea level nor at altitude.

First, we discuss the flammability envelope for Jet-A and the conditions reported in the literature that could enrich the ullage with vapors, rendering it flammable. Next, we present military test data on JP-5 and -8, fuels that are comparable in volatility to Jet-A. The data show that fragment impact (from gun fire) can produce a fuel spray in the ullage that effectively increases the vapor pressure of the fuel making it flammable. These tests produced significant overpressures that would have destroyed the tank. Finally, we summarize the results of a risk assessment study for fuel tank ignition in the Concorde SST by engine debris.

TABLE 3. PERTINENT ACCIDENTS RESULTING IN SEVERED FUEL LINES

Date	Location	Aircraft Model	Event	Damage	Result
6/8/95	Atlanta, GA	DC-9	<ul style="list-style-type: none"> • uncontained engine failure 	<ul style="list-style-type: none"> • debris ruptured a fuel line between the outer fuselage skin and lavatory 	<ul style="list-style-type: none"> • fire destroyed aircraft on ground
7/4/92	Brisbane, Australia	B727-200	<ul style="list-style-type: none"> • shortly after liftoff, first-stage low-pressure compressor of No. 2 engine failed 	<ul style="list-style-type: none"> • debris severed the main fuel line as it separated from the aircraft 	<ul style="list-style-type: none"> • fire ignited and was extinguished by airport fire services after the aircraft completed a circuit
5/3/91	Windsor Locks, CT	B727-100	<ul style="list-style-type: none"> • 9th stage high-pressure compressor disk failed 	<ul style="list-style-type: none"> • debris penetrated the engine nacelle severing the main fuel line 	<ul style="list-style-type: none"> • fuel ignited and burned into the fuselage, igniting the 12,600 lb. cargo (US Mail)
2/17/82	Miami, FL	B727-200	<ul style="list-style-type: none"> • at takeoff, front compressor of front hub in No. 2 engine failed 	<ul style="list-style-type: none"> • debris severed main fuel supply line to No. 2 engine 	<ul style="list-style-type: none"> • fire ignited in engine bay
2/17/76	Denver/ Stapleton	B727-200	<ul style="list-style-type: none"> • No. 2 stage compressor blade separated from rotor 	<ul style="list-style-type: none"> • debris pierced engine case and the adjacent fuel line 	<ul style="list-style-type: none"> • fuel escaping into engine compartment ignited
12/28/75	Gothenburg, Sweden	DC9-40	<ul style="list-style-type: none"> • at takeoff, fan blade came loose 	<ul style="list-style-type: none"> • blade penetrated the compressor case and severed a fuel line 	<ul style="list-style-type: none"> • engine fire ignited and extinguishers had no effect • during spin down a rattling noise came from the throttles
6/28/65	San Francisco, CA	B707-321B	<ul style="list-style-type: none"> • at takeoff, transient loss of operating clearance between 3rd stage turbine disk and inner sealing ring 	<ul style="list-style-type: none"> • debris from 3rd stage turbine disk severed fuel lines 	<ul style="list-style-type: none"> • fuel from fuel line ignited causing explosive separation of portion of lower wing skin

3.1 FUEL TANK ULLAGE FLAMMABILITY.

Many tests and analyses have been conducted on the flammability of the ullage space in an aircraft tank (Nestor, 1967; Pedriani, 1970; Kosvic et al., 1971). Flight conditions were simulated by decreasing or increasing the tank pressure to simulate an aircraft climb or descent, withdrawing fuel to simulate fuel consumption by engine, shaking the fuel tank to simulate aircraft vibration, and heating the fuel to simulate ambient or aerodynamic heating. The ullage space was instrumented to measure temperature, pressure, and composition. The test conditions and results of these studies are summarized in table 4 and discussed below.

3.1.1 Flammability Envelopes under Static (Equilibrium) Conditions.

Under static or equilibrium conditions in an aircraft fuel tank, the fuel vapor/air mixture is mainly determined by the fuel temperature (which establishes the fuel partial pressure) and the altitude (which fixes the total pressure). Comparison of the fuel/air mixture with that required for combustion defines a flammability envelope on a fuel temperature-altitude graph, as illustrated in figure 3. This envelope is bounded on the lower side by a lean limit and on the upper side by a rich limit (solid and dashed curves, respectively). Figure 3 shows this equilibrium (sometimes referred to as static) flammability envelope for Jet-A (or JP-8) and Jet-B (or JP-4). For both types of fuel, the envelope narrows with increasing altitude or decreasing pressure until a pressure limit of flammability is reached at approximately 65,000 ft altitude.

Figure 3 also includes air temperature as a function of altitude for a tropical, standard, and subarctic atmosphere. If these temperature profiles are encountered in flight, it is evident that the formation of flammable vapor/air concentration is essentially limited to a very small portion of a tropical atmosphere for Jet-A and to a somewhat larger portion of a standard atmosphere for Jet-B. Thus, the static or equilibrium flammability envelope in figure 3 suggests that Jet-A can be considered nonflammable for practical purposes. Under actual conditions, however, the fuel temperature may lag the air temperature (because of thermal inertia) and the flammability envelope can be broadened by dynamic and nonequilibrium effects as presented below.

3.1.2 Flammability Envelopes Under Dynamic Conditions.

Dynamic conditions in an aircraft fuel tank can produce important variances from the static (or equilibrium) flammability envelopes discussed above. These variances are a result of dynamic processes such as tank vibration and sloshing (and consequent spray formation), tank breathing, air dissolution, outgassing, and stratification or nonuniformity in vapor concentrations. For example

- a. Vibration can produce a spray (fine droplets or mists suspended in the ullage space). Formation of a spray has no effect on the rich limit of the flammability envelope while it can lower the lean limit if the ignition source occurs within the spray region. Under these conditions, heat from the ignition source evaporates some of the droplets and thus makes an initially-lean region flammable (Nestor, 1967).

TABLE 4. SUMMARY OF KEY STUDIES ON FLAMMABILITY OF AIRCRAFT TANK ULLAGE SYSTEMS

Test Conditions	Nestor (1967)	Pedriani (1970)	Kosvic et al. (1971)
Apparatus	Static tests in 48"-long glass tubes Dynamic tests in 9" dia x 15" L cylinder	23" x 27" x 30" tank	24" dia x 60" L cylinder
Fuel Used	Jet-A, -B, JP-4	JP-4	Jet-A, JP-4, 7
Description of Main Tests	Determine conditions where ignition can be produced by a spark: - Monitor visible flame in static tests - Monitor ΔP , ΔT in dynamic tests	Map fuel vapor concentration profiles with IR sensors	Measure transient fuel vapor concentration at 3 locations with GC/FID
Main Results	Nestor (1967)	Pedriani (1970)	Kosvic et al. (1971)
Flammability Envelopes (FE)	Most important parameters are liquid temperature and ullage pressure		
Nonuniformity in Vapor Concentration Within Ullage	Not measured	- 1% to 2% in static test - Up to 12% in dynamic tests	Generally small except near vents during descent
Dynamics	- Rocking produces slosh and foam that have little effect on FE - Vibration produces spray which lowers lean ignition limit, if ignition source is within spray	Effect of vibration is small compared to liquid temperature and altitude	Vibration increases rate of air off gassing
Aircraft Ascent	Upward shift of both lean and rich limits		Lower fuel/air ratio (equivalent to upward shift of lean/rich limit)
Other Results	- Fuel conditioning has some effect on FE - Blending fuels shift FE significantly		Complex computer models (stratified ullage and evaporative lag) are not very dependable

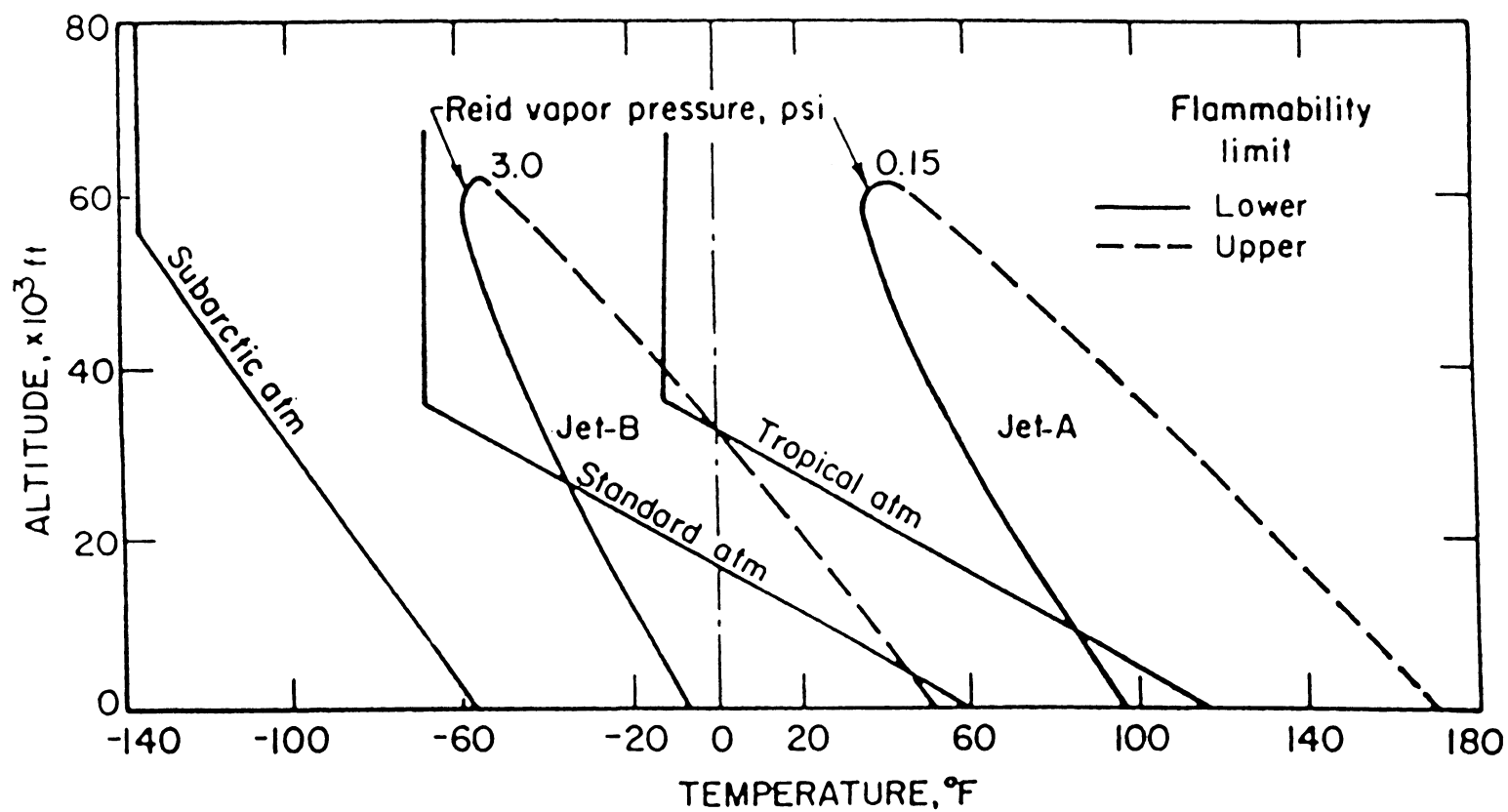


FIGURE 3. PRESSURE ALTITUDE—TEMPERATURE LIMITS OF FLAMMABILITY FOR JET-A AND JET-B TYPE FUELS IN AIR UNDER EQUILIBRIUM (OR STATIC) CONDITIONS (KUCHTA, 1985)

- b. The aforementioned lowering of the lean flammability limit is illustrated in figure 4 by dash-dotted curves for JP-4 (or Jet-B) and JP-8 (or Jet-A) (CRC Report No. 530, 1983). The conventional flammability limits are also shown in figure 4 for reference (solid lines). Note that the lowering of the lean limit is comparable for both fuels.
- c. Vibration increases the off-gassing rate of any air dissolved in the fuel (Kosvic, 1971). The effect of air release on the flammability limits (CRC Report No. 530, 1983) is illustrated in figure 4 by dashed lines. Note that the rich flammability limit is raised, which is understandable, and the lean limit is slightly lowered. (This latter effect is so slight that it can be neglected.) Furthermore, note that the raising of the rich limit is about the same for both Jet-A and Jet-B.
- d. Nonuniformity of the fuel/air concentration can be produced inside the ullage. In one study (Pedriani, 1970), the JP-4 vapor concentration profiles within the ullage varied from 1 to 2 percent (volume vapor in air) in static tests and up to 12 percent in tests with vibration. These are large variations since the flammable range is 1.3 to 8.0 percent. In another study (Kosvic, 1971), the nonuniformities in vapor concentrations were negligible during ascent and level flight but were significant during descent, particularly near vents where air enters the ullage.

In summary, while the static flammability envelope of Jet-A suggests that the ullage of an aircraft tank is not flammable, dynamic considerations indicate significant broadening of the envelope, making the ullage flammable over a wider range of conditions.

In addition to the dynamic conditions discussed above, the impact phenomenon itself can produce a spray that enriches the ullage with vapors. For example, consider a fragment path that enters the tank below the liquid level and exits the liquid into the ullage. The fragment will entrain a spray or mist of fuel. This effect will be discussed in the next section.

3.2 IGNITION AND OVERPRESSURE IN GUNFIRE IMPACT TESTS.

Since there is no data in the literature on fragment impact of fuel tank from uncontained engine failure, we searched for related results in military literature. In-tank fires and explosion from gun fire impact have been of concern in military aircraft. While the energetics of fragments from gun fire are not directly comparable to the case at hand, the results can suggest what sequence of events to expect.

Pertinent gun fire tests are summarized as follows (Botteri, 1966; Kosvic, 1971). A 90-gallon cylindrical, stainless-steel fuel tank was used with provisions for controlling the fuel vapor/air mixture in the ullage and for high-speed photography. Tests were performed with a 4-inch fuel depth, 0.125-inch-thick 2024 T-3 aluminum plate, and standard velocity .50 caliber armor piercing incendiary (API) projected at a 60-degree pitch up and at a 90-degree impact angle. A minimum of five tests were performed with JP-5 and -8 at atmospheric pressure and at various fuel temperatures from 10 to 130°F. Because of the complexity of such tests and the potential for uncontrolled variability in test conditions, such as the exact location of gunfire impact, sufficient repeat tests were conducted to obtain statistically valid results.

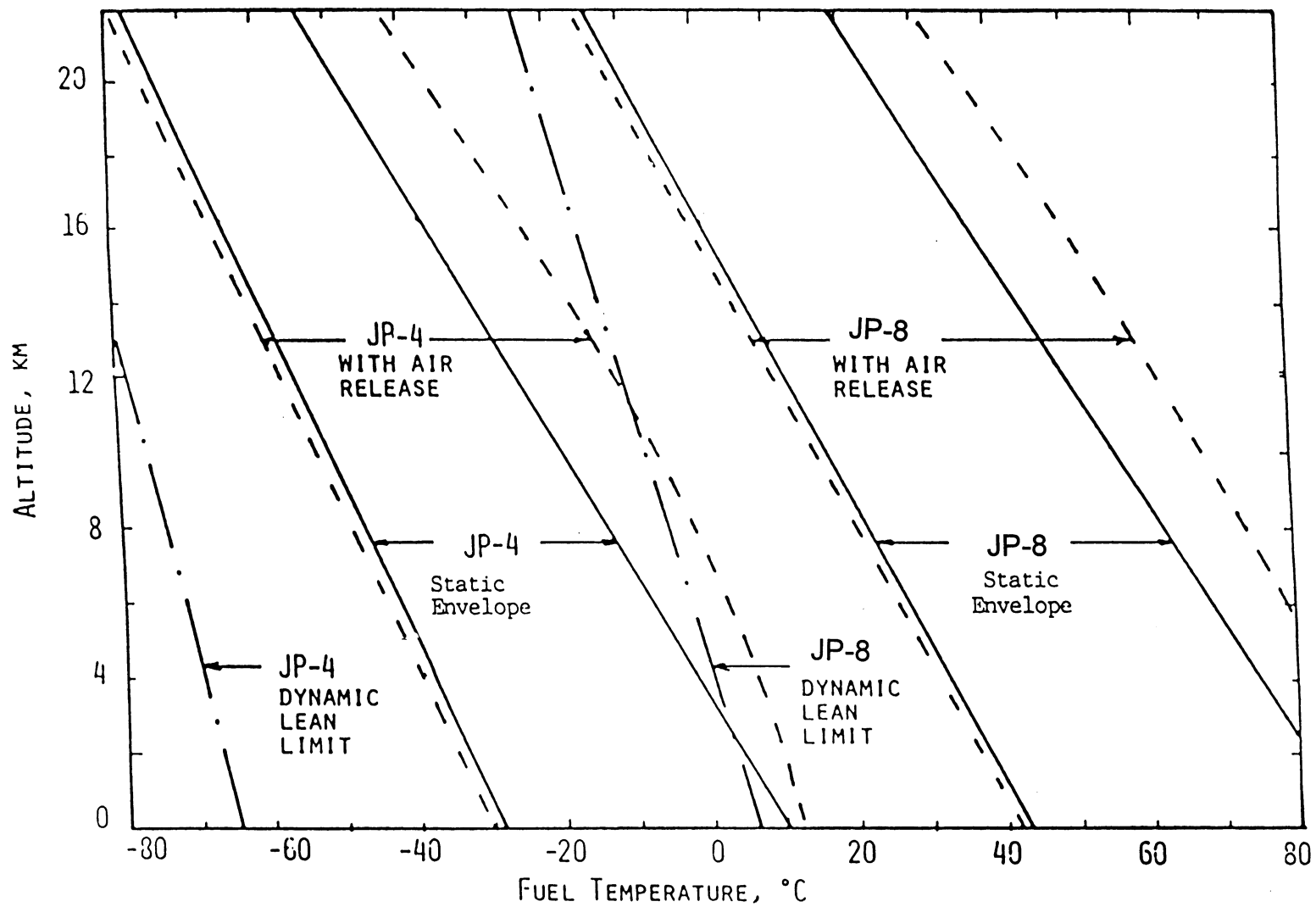


FIGURE 4. FLAMMABILITY LIMITS INCLUDING EFFECTS OF AIR RELEASE AND TANK DYNAMICS
(CRC REPORT NO. 530, 1983)

The combustion overpressure results are presented in figure 5 as a function of initial fuel temperature for each of the fuels separately. Three overpressure values are given: peak, average of reacting tests only (where fuel ignited), and average of all tests (ignition and nonignition). Comparison of these two averages provides a measure of the frequency of ignition. The frequency is high when they are proximate and is low when they diverge. For reference, the overpressure from the API alone, i.e., with no fuel in the tank, was less than 0.8 psi. With fuel, the overpressure for the (ignition) tests exceeded 20 psi (in less than 10 millisec) – even when the fuel temperature was below the flash point by up to 100°F for both JP-5 and -8.

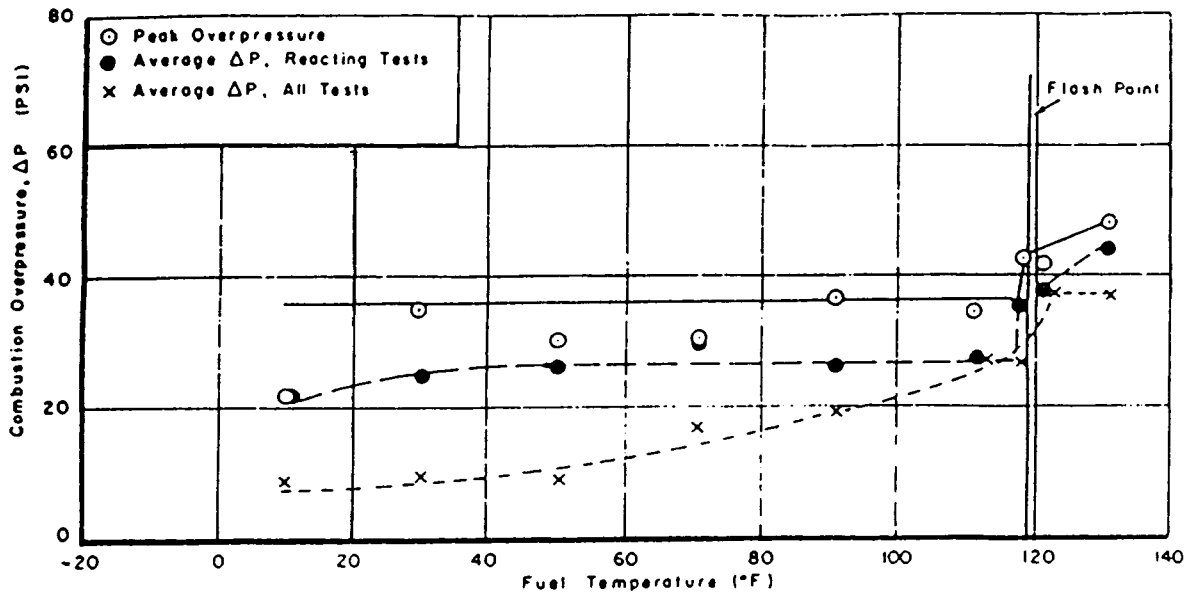
For JP-5 and -8, analysis of high-speed films (7000 frames per second) clearly indicates the formation of fuel mists and sprays due to the impacting projectile which would lower the lean temperature limit. Note that in this region the likelihood of ignition depends on the fuel temperature and increases as the flash point is approached. Given ignition, however, the overpressure is fairly independent of fuel temperature. This can be attributed to a larger mass of fuel in spray than in vapor phase and the dependence of the spray mainly on the projectile impact conditions (which were constant in the tests, Manheim, 1973).

In summary, for the test conditions used, ignition and overpressure under the dynamic conditions of fragment impact simulated by gun fire are possible even with a fuel that is originally below its flash point, i.e., outside the static flammability envelope of the fuel.

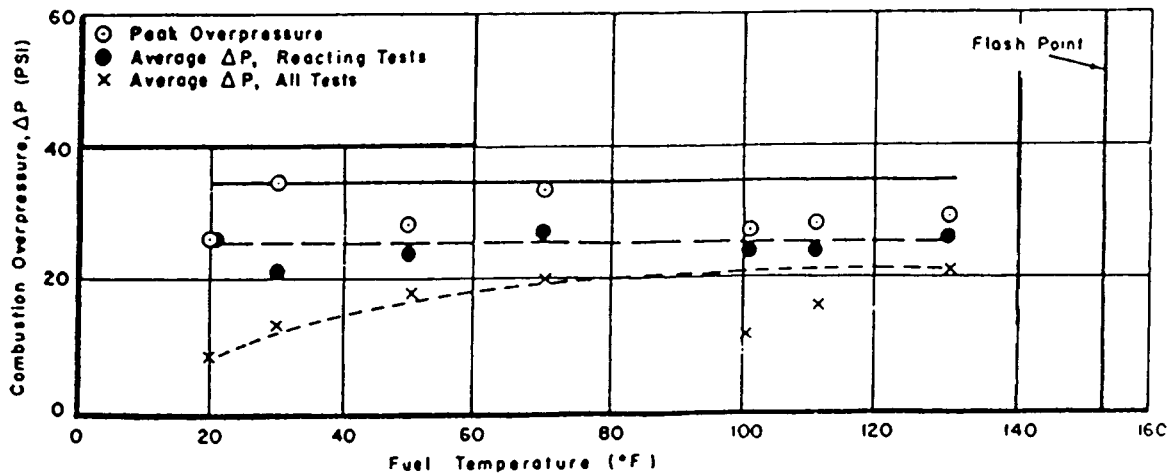
3.3 RISK ASSESSMENT OF IGNITION FOR THE CONCORDE.

Wallin (1976) of British Aerospace developed a methodology to assess catastrophic risks resulting from uncontained failures of turbine engine rotors. This work was undertaken as part of the Concorde SST certification program, using an engine failure model for the Olympus 593. It is summarized in this section because it is the only study we found that recognized the potential hazards of in-tank fire and explosion from uncontained engine failures in commercial aircraft. Wallin began by establishing a hazard tree, evaluating debris size for each engine stage, and determining potential risk items for each stage. A statistical analysis of earlier tests and actual failures provided data for the distribution of risk through each flight stage. A mean catastrophic risk across a typical flight mission was established by summing the overlapping risks using success theory.

Wallin then established a hazard tree for engine rotor failure that included the effects of damage to structure and essential systems, loss of thrust, disturbance of operation, and fires and explosions. The risk assessment included the effects of 1/3 disk pieces and disk rim pieces of 1/2 radius. Such a failure model was adapted from the British Civil Airworthiness Requirements and Olympus 593 failure models that are based on experimental test data and statistics. By examining the structure of the Concorde, Wallin determined the fragment fly-off zone in plan view and established the risk angle associated with each engine stage. In this manner the at-risk items were identified and an overall risk was obtained for each flight phase.



JP-8



JP-5

FIGURE 5. COMBUSTION OVERPRESSURE AS A FUNCTION OF FUEL INITIAL TEMPERATURE FOR GUNFIRE TESTS FOR JP-5 AND -8 (90-GALLON TANK, 4-INCH FUEL DEPTH AT ATMOSPHERIC PRESSURE)

Wallin (1976) calculated the mean probability of catastrophic aircraft loss using

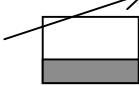
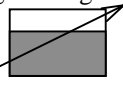
$$probability = (T_R \times I_R \times H_R \times L_R) + E_R \quad (2)$$

where T_R is the proportion of flight phase where fuel is present in the penetrated tank, I_R is the ignition probability, H_R is the probability of the fire situation becoming catastrophic, L_R is the probability of not landing safely with a catastrophic fire, and E_R is the probability of a catastrophic explosion at the instant of penetration. The first term (in parentheses) is the probability of loss of aircraft due to fire caused by fuel tank penetration.

Wallin established an ignition probability for both fires and explosions, which had a significant impact on the overall risk assessment. Wallin notes that the values used were derived from the original Civil Aviation Authority (CAA) guideline but stressed that they should be treated with some reserve, since they were derived from military experience with missiles.

Wallin's probabilities of ignition due to penetration of fuel tanks by hot engine debris are summarized in table 5. For the case of fragments that enter the ullage above the fuel level, he assigned (based on judgment) an 80 percent probability of an explosion when the fuel temperature is within the flammability limits. For the case of fragments that pass through the liquid prior to entering the ullage, a 70 percent probability is assigned when the fuel temperature is within flammability limits. For the mist region, Wallin approximated the risk by assuming arbitrarily a 5 percent probability of ignition at -50°C , which rises linearly to 70 percent at the lean limit.

TABLE 5. THE IGNITION RISK FACTORS FROM WALLIN (1976)

Fuel Conditions in Ullage Space	Ignition Probability	
	Mist by Fragment ($T < T_{lean}$)	Temperature (T) Within Flammability Limits *
Penetration Scenario		
Fragment enters ullage above liquid 	N/A	80%
Fragment enters ullage through liquid 	5% @ $T = -50^\circ\text{C}$ rising linearly to 70% at T_{lean}	70%

*dependent upon the flight profile

It is ironic, therefore, that a postscript to Wallin's report recommended that the ignition risk factor be eliminated, a drastic step which would eliminate an entire branch of the hazard tree.

Our work in section 4 indicates that, in fact, the hazard of fire or explosion is possible, which corroborates Wallin's report.

4. POTENTIAL FUEL TANK IGNITION BY ENGINE DEBRIS.

This section investigates two scenarios that may lead to ignition of the fuel as illustrated in figure 6. The first scenario occurs when a fragment enters the tank and travels through the air space above the free surface of the liquid fuel, referred to as the ullage. An analysis of the convective heat transfer from the fragment to the ullage gases permits us to determine the temperature of the fragment and its surrounding vapor film as a function of time. Then we compare the temperature-time history of this film to that required for fuel ignition as measured in fundamental studies by Spadaccini and TeVelde (1982).

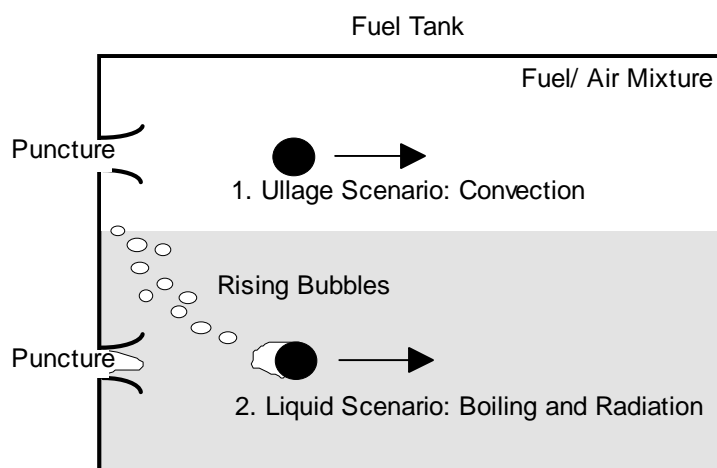


FIGURE 6. TWO SCENARIOS OF FRAGMENT ENTERING FUEL TANK

In the second scenario, the fuel is heated as the hot fragment enters and travels through the fuel tank within the liquid portion only. An analysis similar to that of the ullage is carried out with the addition of boiling and radiative heat transfer from the fragment. We also consider the motion of the vaporized fuel as bubbles rise to the free surface of the fuel tank, where it may ignite the vapor in the ullage. Ignition may take place within the bubble as it rises or when it hits the free surface depending on the rate of heat transfer.

A combination of these two scenarios occurs when the fragment enters the liquid and traverses through it to the ullage space or vice versa. We will consider this combination by examining the results of the two separate scenarios.

The fragment used in the analysis of this section is a typical blade from the turbine section where the temperature is high, and consequently, the potential for ignition is high. In addition, the friction forces of impact can further heat up a fragment. This effect is examined in an exploratory way in appendix B. Our results suggest that friction can increase the temperature of either cold or hot fragments significantly. Because these results are preliminary, we have not taken this increase into account in this section.

The heat transfer analysis will indicate whether the temperature of the vapor film reaches ignition conditions. In addition, for the fuel to ignite, the surrounding fuel/air mixture must be in the flammable range. We will calculate the concentration of fuel in the wake of the fragment in order to refine our assessment of the likelihood of ignition. For the case of fire in the ullage, we account for the evaporation of droplets produced by agitation of the tank that increases the concentration of fuel. For the liquid case, we calculate the amount of fuel vaporized and consider the amount of air entrained within the fragment's wake.

This section first describes the temperature-time history required for ignition of a fuel/air mixture, then the analysis of each scenario of ignition is presented separately describing the heat transfer modes, temperature profile, and examining the fuel/air mixture.

4.1 TEMPERATURE-TIME REQUIREMENTS FOR IGNITION.

The conditions favorable for ignition of a combustion process by a hot fragment depend on the fuel/air mixture, temperature of the fragment, the flow velocity, and the exposure duration to the hot fragment. Johnson et al. (1988) studied the effect of a hot surface on the ignition of aircraft fuels. Ignition occurs when the exposure duration exceeds an ignition delay time (also called ignition time) characteristic of the fuel. They used a one-step second order reaction to model the kinetic portion of the ignition delay time (t_c) an Arrhenius equation given by

$$t_c = f \cdot \exp\left(\frac{E_a}{\Re T}\right) / p^n \quad (3)$$

where f is the pre-exponential factor, E_a is the activation energy, p is the pressure, \Re is the universal gas constant, T is the absolute temperature, and n is the order of the reaction. Spadaccini and TeVelde (1982) fit this equation to data from a continuous flow experiment using various aircraft-type fuels injected as a spray. They found that the data fit this relation for JP-8 with an activation energy of 37.78 kcal/mole and a pre-exponential factor of 1.68×10^{-8} ms/atm² and $n = 2$. Their experiment was performed at pressures between 10 and 30 atm. We are interested in ignition at atmospheric and subatmospheric pressures and therefore need to verify this relation and fitting parameters for the range of pressures of interest.

Spadaccini (1977) studied the effect of elevated pressure on the ignition characteristics of hydrocarbon fuels. By extrapolating his data to the results at atmospheric pressure of Mullins (1953), Spadaccini determined that the pressure dependence can be accounted for by a pre-exponential factor that is inversely proportional to p^2 , consistent with equation 3.

The procedure for performing continuous flow experiments requires increasing the temperature of the free stream until ignition occurs at the end of the test section. The ignition delay time is equated to the residence time within the test section, which is the ratio of test length to flow velocity. By varying the test length and flow velocity at various pressures, Spadaccini and TeVelde (1982) obtained a full range of ignition delay times. When making these measurements for short test sections, however, the flow velocity had to be reduced. As a result, the hot stream and injected fuel did not have the same mixing characteristics as experiments with larger velocities or test sections. The resulting nonuniformities tended to increase the likelihood of ignition for the conditions of poor mixing.

The data of Spadaccini and TeVelde (1982) showed that this mixing effect is important for high temperatures and the lower end of their pressure range. We are interested in applying their results for temperatures below 850 K. Spadaccini and TeVelde showed that, for temperatures below 825 K, data (obtained under different mixing conditions) collapse in one curve when plotted as $t_c p^2$ versus $1/T$. Furthermore, we expect to have a high degree of mixing due to the high velocity and external flow around the moving and turning turbine fragments. Because of the low temperature and the high mixing, we can apply the results of Spadaccini and TeVelde to the condition of atmospheric pressure for temperatures below 825 K without significant error.

4.2 FRAGMENT MOTION.

Fragments resulting from catastrophic engine failure vary in size and shape. Fragments may be sections of fan and compressor blades weighing less than 1/3 kg moving at 350 m/s or as large as disk and rim sections weighing more than 80 kg moving at 50 m/s. Small fragments can have a wide range of geometries depending on the manner of the break up. The geometry of the fragments varies from thin blades to circular sectors of more complex shape. For subsequent calculations in this section, we will focus on a typical blade from the high pressure turbine. The blade is assumed to operate at 7200 RPM, have a mass of 0.059 kg, a length of 0.17 m, and a fragment velocity of 237 m/s (Mattingly et al., 1987, and engine specifications from CFM International, 1996).

For our analysis, the fragment geometry was simplified to enable the use of standard correlations for heat transfer and drag coefficients from the literature. We assumed that the fragment was a cylinder in cross-flow. Our interest in determining the regime for ignition justifies this geometric simplification since we are estimating only the regime boundary between ignition and no ignition for a representative fragment.

The fluid drag forces will slow down the fragment as it passes through the stagnant fluid in the tank. The sum of the forces on the fragment equals:

$$m \frac{dV}{dt} = -F_D = -A_f C_D \rho \frac{V^2}{2} \quad (4)$$

where m is the mass of the fragment, V is its velocity, F_D is the drag force, C_D is the drag coefficient, ρ is the fluid density, and A_f is the area of the fragment perpendicular to the flow. For Reynolds numbers ($Re_D = \rho V D / \mu$, where μ is the viscosity of the fluid) greater than about 400, the drag coefficient is approximately unity for a smooth cylinder (Incropera and DeWitt, 1985). We are interested in the first few moments after the fragment enters the tank, when the Reynolds number is very large. For a cylinder, the area is $\pi D L$, where D is the cylinder diameter and L is its length. Integrating equation 4, assuming that the drag coefficient is constant, yields an expression for the velocity:

$$V(t) = \frac{V_o}{1 + \frac{DLC_D \rho}{2m} V_o t} \quad (5)$$

Where V_o = the initial fragment velocity. Figures 7 and 8 show the velocity and travel distance for the typical blade fragment defined above modeled as a cylinder traveling in the ullage and in the liquid fuel, respectively. Each figure plots the change in velocity and time as the fragment travels one meter, a typical fuel tank size. The fragment does not slow down appreciably while traversing the ullage, while it slows down very quickly in the liquid because of the liquid's higher density. According to equation 5 the time constant for velocity decay is

$$\tau = \frac{2m}{DLC_D \rho_l V_o} = 0.5 \text{ msec for the liquid.}$$

4.3 FRAGMENT ENTERING ULLAGE.

As mentioned, ignition requires both a sufficient temperature and fuel/air mixture. First, we examine whether the fragment is hot enough to heat the vapor to the temperature required for ignition and maintain it at that temperature for the duration of the ignition delay time. Next, we examine whether the fuel/air mixture is within the flammability range. Examination of these two requirements for ignition is done separately to make the problem tractable. All the properties used for the calculations in this section are given in tables 6 and 7.

4.3.1 Heat Transfer.

Consider a fragment that penetrates the fuel tank and travels through the ullage of the fuel tank. The flux of energy, q'' (in W/m^2 , Watts per square meter), transferred to the vapor is given by

$$q'' = h(T - T_\infty) \quad (6)$$

where T is the temperature of the surface, T_∞ is the temperature of the free stream, and h is the heat transfer coefficient ($\text{W/m}^2 \text{ K}$) due to convective heat transfer. For the case of convective heat transfer, Incropera and DeWitt (1988) give the following relationship for the heat transfer coefficient for cylinders in cross-flow:

$$h_{conv} = \frac{k}{D} \left[0.3 + \frac{0.62 \text{Re}_D^{1/2} \text{Pr}^{1/3}}{\left[1 + (0.4/\text{Pr})^{2/3} \right]^{1/4}} \left[1 + \left(\frac{\text{Re}_D}{28,200} \right)^{5/8} \right]^{4/5} \right] \quad (7)$$

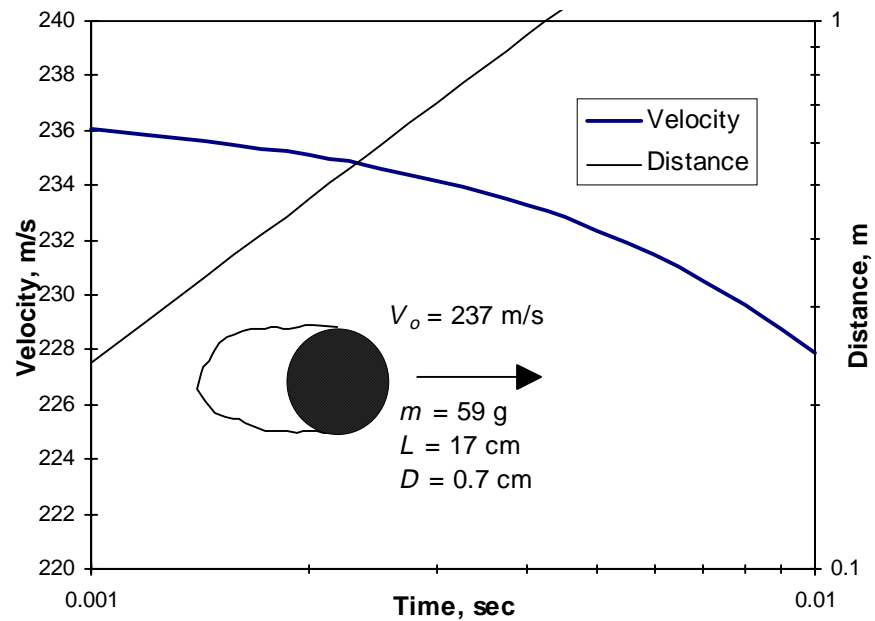


FIGURE 7. VELOCITY AND DISTANCE OF TYPICAL INCONEL FRAGMENT TRAVELING THROUGH ULLAGE; INITIAL $Re_D = 6.8 \times 10^4$

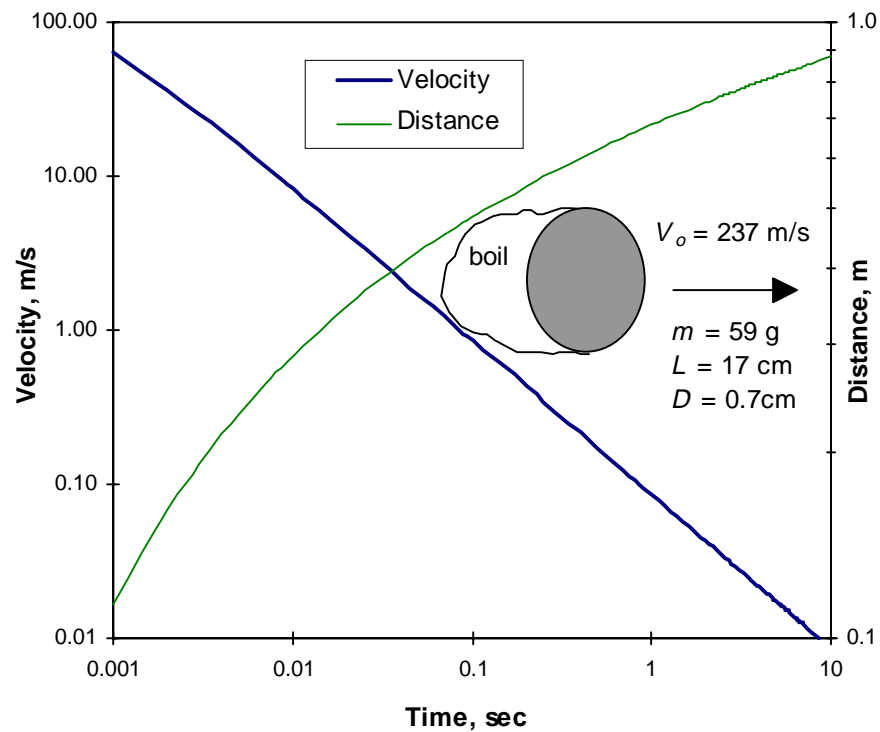


FIGURE 8. VELOCITY AND DISTANCE OF TYPICAL INCONEL FRAGMENT TRAVELING THROUGH LIQUID FUEL; INITIAL $Re_D = 1.4 \times 10^6$

TABLE 6. PROPERTIES OF JET-A FUEL

Liquid Properties (from Moussa, 1980 unless otherwise indicated)			
viscosity	0.0013 kg/(m s)	Saturation Temperature at 1 atm, T_{sat}	459 K
density	800 kg/m ³	thermal conductivity Perry (1950)	0.145 W/(m K)
surface tension	0.028 N/m	Prandtl Number	17
heat of vaporization	291 kJ/kg	molar mass Johnson et al. (1988)	167 g/gmole
Vapor Properties			
characterization factor Perry (1950)	11.79	thermal conductivity Maxwell (1950)	$8.1 \times 10^{-5} T - 0.014$ W/(m K)
specific heat Maxwell (1950)	$3.01 \times T + 729$ J/(kg K)	viscosity Maxwell (1950)	$1.18 \times 10^{-8} T + 1.28 \times 10^{-6}$ kg/(m s)

TABLE 7. PROPERTIES OF DISK FRAGMENT MATERIALS FROM INCROPERA AND DE WITT (1985)

Property	Titanium	Inconel X-750
density (kg/ m ³)	4500	8510
heat capacity (J/kg)	$166.12 T^{0.1987}$	$81.405 T^{0.2905}$
thermal conductivity (W/(m K))	$1 \times 10^{-5} T^2 - 0.0171 T + 26.417$	$0.5728 T^{0.5346}$

where k is the thermal conductivity of air, Pr is the Prandtl number, and the Reynolds number (Re_D) is evaluated at the fragment velocity and the film temperature. This correlation is valid for $Re_D Pr > 0.2$; $Pr = 0.707$ for air. Using the velocity given by equation 5, we calculate Re_D and thus the heat transfer due to convection by equations 6 and 7.

We calculate the temperature of the fragment by noting first that the high thermal conductivity of the fragment permits us to neglect any temperature gradients within the fragment. The temperature of the fragment is obtained by using equation 6 with

$$q'' = -\frac{mc}{\pi DL} \frac{dT}{dt} \quad (8)$$

where c is the specific heat of the fragment. The results are presented in the next section.

4.3.2 Film Temperature-Time History Versus Ignition Requirements.

In this section we calculate the vapor film temperature-time history in the wake of the hot fragment and compare it with that required for ignition as discussed in section 4.1. Very close to the fragment surface, the film temperature is nearly the same as the fragment. Moving away from the surface, it decays to the ambient temperature. For this calculation the film temperature is assumed equal to the fragment temperature. This assumption is justified, since in a nonuniform temperature region, it is the highest temperature that causes ignition, as shown by Spadaccini and TeVelde (1982). The ignition time should be less than the transit time of the fragment inside the ullage. Ignition may fail because the vapor film is not heated to a sufficiently high temperature or for a sufficiently long time.

Figure 9 shows the film temperature next to the hot fragment as a function of time for a fragment of 59 g with an initial velocity of 237 m/s. The temperature history of two types of fragments, titanium and Inconel, are shown. These two materials have different initial temperatures and cool down rates, the latter difference caused by differences in specific heat and density. The required time for ignition, equation 3, as a function of temperature is also shown. Mattingly et al. (1987) indicates that titanium is used up to operating conditions near 700 K, while Inconel is used up to 1400 K. (In an uncontained engine failure, the initial blade temperature can be higher than normal operating temperatures, but we did not account for this effect.) Our analysis shows that under normal conditions turbine blades of titanium are not hot enough to produce ignition. The Inconel fragments, however, show a greater likelihood for igniting the fuel. (The most advanced engines use Rene 80 at even higher operating temperatures.) For an initial velocity of 237 m/s, the fragment travels 1 m in the ullage within 4 msec (see figure 7). We assumed that 1 m is a characteristic length of the tank, and therefore use 4 msec as a cutoff to indicate that the fragment will no longer be in the tank. This cutoff shows that for initial temperatures greater than 986 K, the fragment will raise the film temperature high enough for ignition as shown by the three curves for an Inconel fragment at different initial temperatures in figure 9. The shaded wedge region in figure 9 is where ignition occurs because both temperature and time requirements are satisfied.

We have analyzed the effect of pressure on ignition. For an aircraft traveling at an altitude of 10,000 m, where the pressure is 0.26 atm, the ignition delay time is longer. In addition, the ambient temperature and fuel density are less than those at sea level. The temperature-time characteristics at the lower pressure at 10,000 m are shown in figure 10. Under these ambient conditions, an Inconel fragment will reach the 1 m characteristic length in 0.2 msec. As a result, ignition will only occur for initial fragment temperatures greater 1370 K, which is still within the normal operating temperatures of the turbine, but marginally. Thus, the shaded wedge region denoting ignition is much smaller at altitude than at sea level.

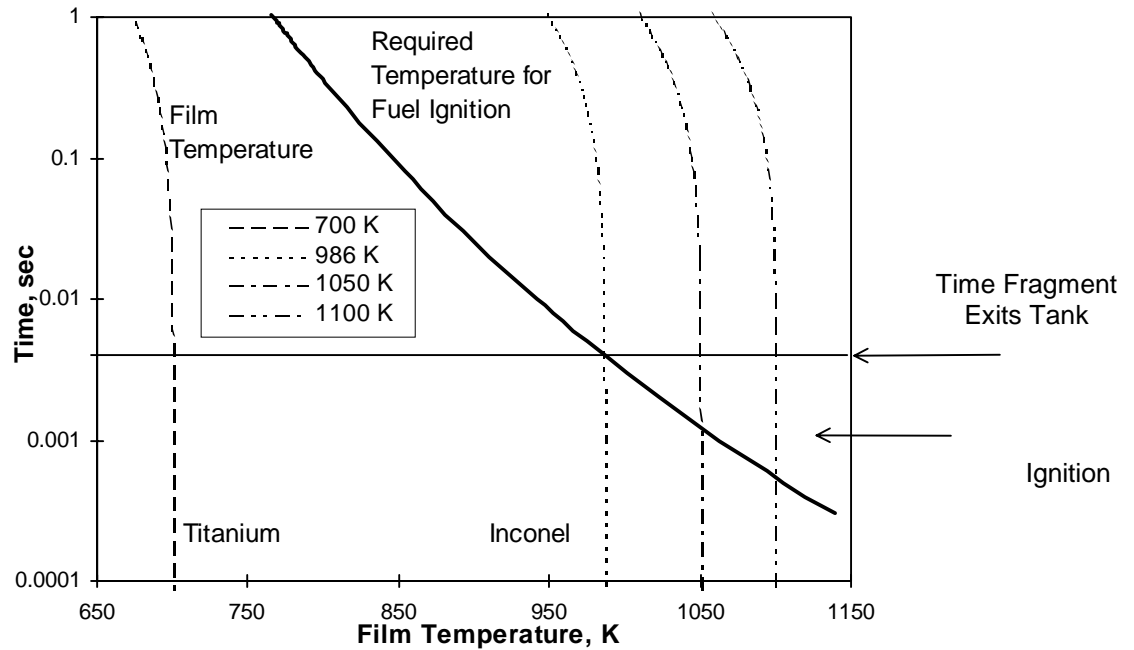


FIGURE 9. TEMPERATURE-TIME HISTORY OF FILM AROUND FRAGMENT AND TEMPERATURE-TIME REQUIRED FOR IGNITION IN ULLAGE AT SEA LEVEL ($V_o = 237$ m/s, 59 g FRAGMENT)

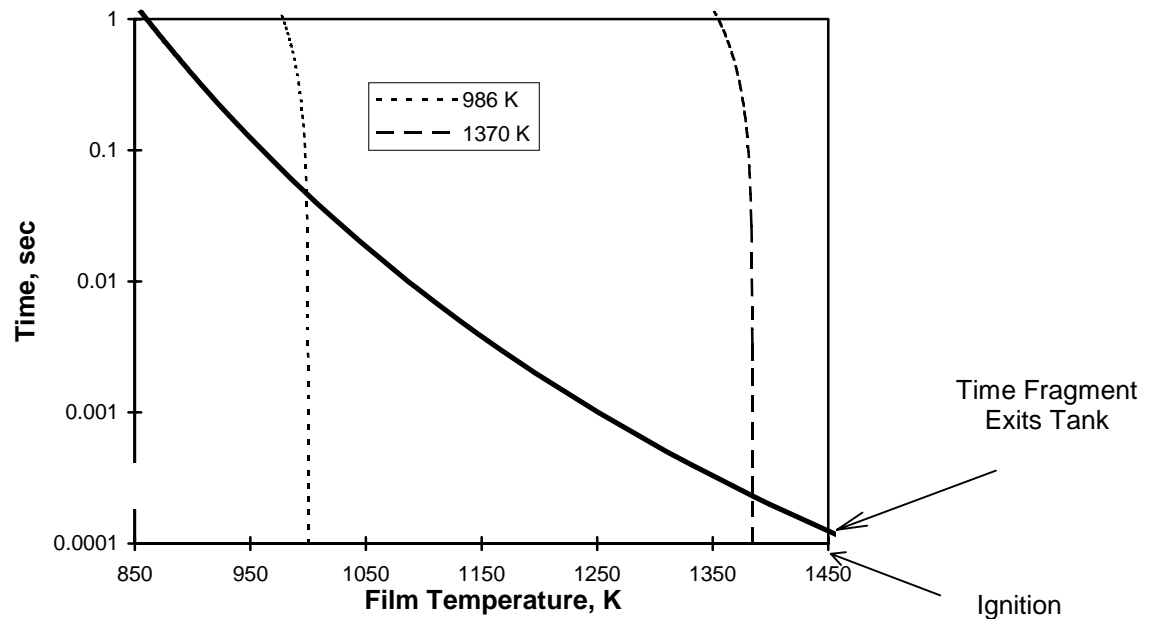


FIGURE 10. FILM TEMPERATURE-TIME HISTORY AND TEMPERATURE-TIME REQUIRED FOR IGNITION IN ULLAGE AT AN ALTITUDE OF 10,000 m ($V_o = 237$ m/s, 59 g INCONEL FRAGMENT)

4.3.3 Fuel/Air Mixture.

We have evaluated the thermal conditions that determine fuel ignition by a hot fragment. In order for the fuel to ignite, it must not only be hot enough, but there must also be a required mixture of fuel and air to permit combustion. This section presents an analysis of the concentration of the fuel near the fragment to determine if the mixture can ignite.

Consider a fragment that enters the ullage of the tank. The concentration of vapor is low, but due to sloshing of the liquid fuel, small droplets of liquid are present in the ullage. As the hot fragment traverses the tank, it will vaporize any droplets that it encounters. The vapor will enter the wake of the fragment where it increases the air/fuel mixture and may lead to the appropriate conditions for ignition. In the following discussion, the wake refers to the region directly behind the projectile, which is on the order of several diameters of the fragment. This region moves with the fragment.

Assume a uniform distribution of droplets of diameter, d , in front of the fragment, spaced a distance S apart. The number density of droplets, therefore, is $1/S^3$, and the number of drops intercepted by the fragment is

$$N = \frac{xDL}{S^3} \quad (9)$$

where x is the fragment travel distance (integral of the velocity given by equation 4). If the fragment vaporizes all the drops it contacts, the mass and density of the vapor in the wake can be estimated from a mass balance, including the vapor already present in equilibrium.

$$m_{vap} = m_{drops} + m_v = \rho_l \left(\frac{\pi d^3}{6} \right) N + \frac{p_v \hat{M}_v}{\Re T} (S^3 N) \quad (10)$$

where p_v is the fuel vapor pressure, \hat{M}_v is the fuel molecular weight, \Re is the universal gas constant, and the density of the liquid fuel (droplets) is evaluated at atmospheric conditions. We can define the void fraction, ε , of the initial distribution of droplets by

$$\varepsilon = \frac{S^3 - \frac{\pi d^3}{6}}{S^3} = 1 - \frac{\pi}{6} \left(\frac{d}{S} \right)^3 \quad (11)$$

As a result, the mass (m_{vap}) and concentration χ_{v_∞} of the fuel far downstream of the wake depends only on the initial droplet distribution

$$m_{vap} = \left[\rho_l (1 - \varepsilon) + \frac{p_v \hat{M}_v}{\Re T} \right] (xDL) \quad (12)$$

$$\chi_{v_\infty} = \frac{\frac{m_{vap}}{\hat{M}_v}}{\frac{m_{vap}}{\hat{M}_v} + \frac{\rho_{air} Vol_{air}}{\hat{M}_a}} = \frac{\frac{\rho_l(1-\varepsilon)\mathcal{RT}}{\hat{M}_v} + p_v}{\frac{\rho_l(1-\varepsilon)\mathcal{RT}}{\hat{M}_v} + p_v + p_a} \quad (13)$$

The infinity in the subscript denotes the concentration of fuel vapor far downstream of the wake where the fuel is not being pulled along with the fragment.

In equation 13, the term involving the void fraction ($\rho_l(1-\varepsilon)\mathcal{RT}/\hat{M}_v$) resembles a relation for an ideal gas with the exception that the density is for liquid weighted by a fraction, $(1-\varepsilon)$. This term is an effective vapor pressure of the suspended drops due to sloshing of fuel in the tank, assuming that they evaporate completely due to heat transfer from the fragment. These drops will have a particular size and distribution depending on the nature of the agitation and the physical size of the tank and ullage. We can estimate this effective vapor pressure (which we call p_{drops}) by examining test data from the study of the effects of tank dynamics on the flammability limits of aviation fuels.

The flammable concentration range of Jet-A is 0.6% to 4.7% (Moussa, 1990). In other words, at the lower flammability limit, the fuel mole fraction at ignition, $\chi_{ignition}$ is 0.6%. Using the above definition of p_{drops} , equation 13 can be rewritten at ignition as

$$\chi_{ignition} = \frac{p_v + p_{drops}}{p_v + p_{drops} + p_{air}} = 0.6\% \quad (14)$$

Therefore,

$$p_{drops} = 0.006p_{air} - p_v \quad (15)$$

Dynamic conditions within a fuel tank decrease the temperature required for ignition at the lean end of the flammability envelope (as presented in figure 4). This effect can be related to the effective vapor pressure of the drops as illustrated in table 8. The calculation assumes that the minimum fuel concentration required for ignition of Jet-A is 0.6% independent of pressure. Note that under static conditions $p_{drops} = 0$ as expected. On the other hand, under dynamic conditions p_{drops} is significantly larger than p_v indicating that most of the fuel in the ullage is in the form of droplets. For temperatures higher than those listed, the mixture has a composition greater than the lean flammability limit.

Near the fragment the concentration of the fuel is higher due to the evaporation of the droplets by the fragment. The boundary layer has a very high concentration of fuel, because it is the location of droplet vaporization. Far behind the wake, the concentration can be high enough to promote ignition. In the wake itself, the concentration varies due to mixing of the hot air near the fragment and the quiescent fluid. The concentration must decrease in some manner from the boundary layer to the downstream value. Because the downstream value is lean, there will be

regions for which the concentration is high enough for ignition during the entire time the fragment traverses the ullage.

In conclusion, ignition in ullage can occur for fuel tanks involving agitation and for a range of flight altitudes.

TABLE 8. EFFECT OF TANK DYNAMICS ON FLAMMABILITY LIMITS

Altitude	Condition	Minimum Temperature Required for Ignition, K	Vapor Pressure p_v , Pa	Effective p_{drops} , Pa
m.s.l. P=1 atm	static	315	607.9	-
	dynamic	278	61.4	546.5
10,000 m P=0.26 atm	static	288	158.1	-
	dynamic	268	38.4	119.6

4.4 FRAGMENT ENTERING LIQUID FUEL.

4.4.1 Heat Transfer From Fragment.

We will examine heat transfer by three modes: forced convection, boiling, and radiation across the vapor film near the fragment surface. For convection, the heat transfer coefficient is given by equation 7, where we use the liquid properties of the fuel, k is the thermal conductivity of the liquid fuel, and the Reynolds number is evaluated at the fragment velocity and the film temperature. This correlation is valid for $Re_D Pr > 0.2$; $Pr = 17$ for kerosene. Using the velocity given by equation 5, we calculate Re_D and thus the heat transfer due to convection by equations 6 and 7.

The pool boiling curve describes the mode of heat transfer that occurs from a hot body submerged in a liquid at saturated conditions (Incropera and DeWitt, 1988). When the body temperature is greater than the saturated vapor temperature ($T - T_{sat} > 30$ K), film boiling predominates the heat transfer (otherwise nucleate boiling predominates). For our case, this temperature difference starts at: $T - T_{sat} > 241$ K. Under film boiling conditions, the heat transfer coefficient is given below (Incropera and DeWitt, 1988).

$$h_{film} = 0.62 \frac{k_v}{D} \left[\frac{g(\rho_l - \rho_v) h'_{fg} D^3}{\nu_v k_v (T - T_{sat})} \right]^{1/4} \quad (16)$$

where k is the thermal conductivity of vapor, ν the kinematic viscosity, ρ is the density and $h'_{fg} = h_{fg} + 0.4 c_{p,v} (T - T_{sat})$, where c_p is the specific heat, and h_{fg} is the heat of vaporization. The subscript v denotes a property of the vaporized fuel evaluated at the arithmetic mean of the surface temperature, T , and the saturated vapor temperature, T_{sat} . The subscript l denotes a property of the liquid.

At elevated temperatures, the radiation across the film from the hot surface to the liquid fuel must be considered. When the heat transfer coefficient for radiation is less than that due to boiling, a simplified correction to equation 16 accounts for radiation across the film (Incropera and DeWitt, 1985)

$$h_{rear} = h_{film} + \frac{3}{4}h_{rad} \quad \text{where} \quad h_{rad} = \frac{\epsilon \sigma (T_s^4 - T_{sat}^4)}{T_s - T_{sat}}. \quad (17)$$

where ϵ is the emissivity (approximately $\epsilon = 0.3$ for non-shiny metals, Incropera and DeWitt, 1985) and σ is the Stephen-Boltzmann constant, and T_s is the surface temperature of the fragment.

4.4.2 Temperature Profile.

As the fragment enters the fuel tank, the fragment cools at a spot (T_l) on the leading edge of the fragment (see inset of figure 11). The Reynolds number is extremely high, producing rapid convective cooling of the leading edge. In the recirculation zone behind the fragment, boiling will occur.

We can model the fragment as an infinite two-dimensional cylinder with idealized boundary conditions. We consider that the front of the cylinder is cooling by convection to a stream at velocity V , and the back surface cools by film boiling. We can use equation 16 to estimate the heat transfer coefficient by assuming that pool boiling conditions exist; i.e., there is no forced convection in the vapor pocket trailing the fragment. We expect any forced convection or mixing will increase the heat transfer and reduce the fragment temperature more quickly.

We can divide this idealized fragment into a number of regions and use a finite-difference approach to solve for the temperature profile across the cylinder. For this problem, there are two Biot numbers describing the rate of heat transfer at the front and rear surfaces of the cylinder, normalized by heat conduction inside the cylinder

$$Bi_1 = \frac{h_{conv}\Delta x}{k} \quad Bi_2 = \frac{h_{rear}\Delta x}{k} \quad (18)$$

The Fourier number (normalized heating time) is

$$Fo = \frac{k\Delta t}{\rho c(\Delta x)^2} \quad (19)$$

where Δx and Δt are spatial and time steps in integration, respectively.

We assume that the entire leading half of the circumference (front face of our idealized fragment) cools by convection and the rear half (back face) by boiling with radiation. Stepping through time to satisfy the convergence criteria $Fo(1 + Bi) \leq \frac{1}{2}$, yields a temperature profile across the fragment for each time step. Figure 11 illustrates the temperature at three points across the cylindrical fragment for the case of a 0.7 cm diameter cylinder with a mass of 59 g and an initial

velocity of 237 m/s; typical values for a fragment of a turbine blade. This analysis assumes an Inconel turbine part with an initial temperature of 1343 K entering the tank with a fuel temperature at 300 K.

The profile shows that, indeed, the fragment will cool rapidly at the leading surface (T_1) and less quickly at the trailing side (T_3) where the heat transfer coefficient due to boiling is smaller. Because of the drag force on the fragment, it slows very quickly, and the heat transfer will also reduce. The fragment, however, is still hot at its center, (T_2), which causes reheating of the leading edge as the fragment rapidly slows down (decreasing the rate of convective cooling). We are interested in ignition conditions, and therefore the trailing edge is the point to examine in order to determine whether ignition occurs. It is the cooling of this point and the heating of the vapor adjacent to it that we will compare to the ignition delay time in order to assess the likelihood of ignition.

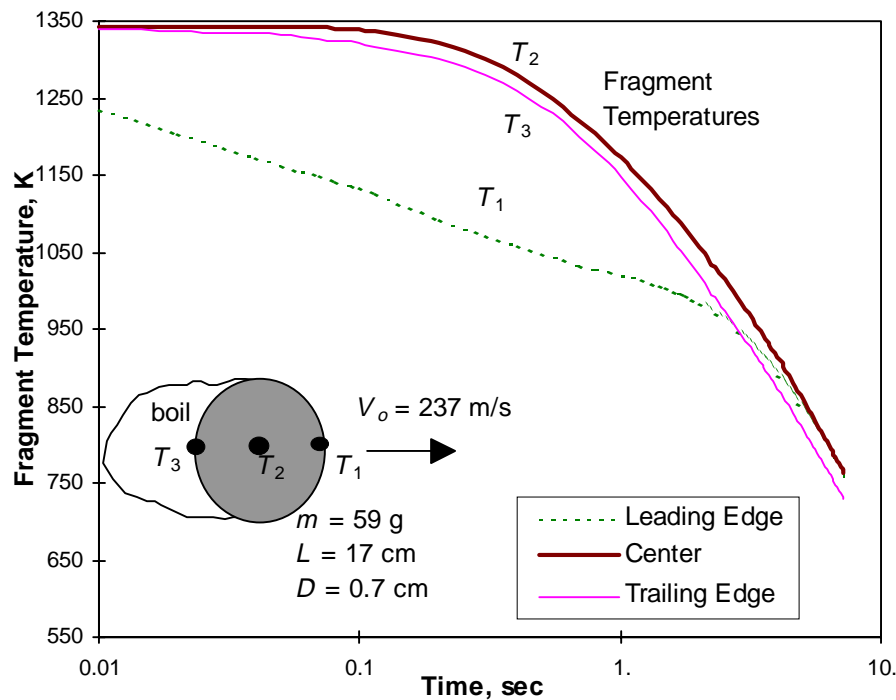


FIGURE 11. TEMPERATURE PROFILE OF INCONEL FRAGMENT TRAVELING THROUGH LIQUID KEROSENE

4.4.3 Film Temperature-Time History Versus Ignition Requirements.

In the liquid fuel, the fragment slows down significantly and its residence time in the tank increases (to the order of one second). See figure 8. Ignition is then predicated mainly on the film temperature.

Figure 12 shows the film temperature next to the trailing edge of the fragment as a function of time. The film temperature is approximated by half the sum of the surface temperature and the liquid temperature. Also shown in figure 12 is the curve for the required temperature for ignition

obtained from equation 3. As before, figure 12 includes the results for two initial fragment temperatures, one representative of a titanium fragment and one for an Inconel fragment, with a mass of 59 g and a length of 17 cm.

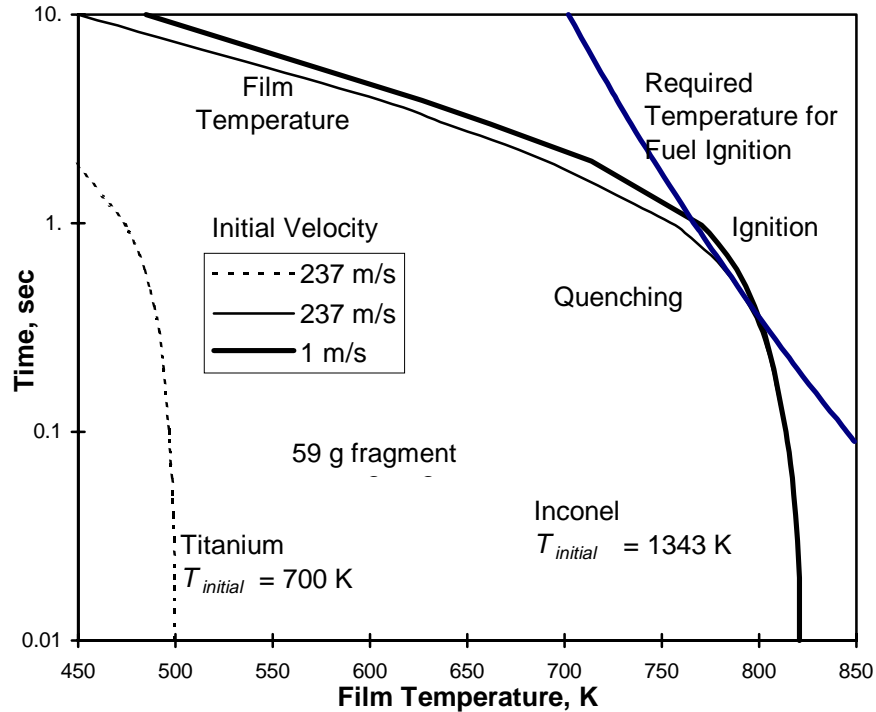


FIGURE 12. TEMPERATURE-TIME HISTORY OF VAPOR AT BOILING SURFACE AND TEMPERATURE-TIME REQUIRED FOR IGNITION IN LIQUID FUEL

The results indicate that for a turbine blade of titanium ignition should not occur in the vapor being produced by the hot fragment because titanium blades are not subjected to high enough operating temperatures. For Inconel parts that operate at higher temperatures, there is a greater possibility of ignition, and there is little effect of changing velocity. A temperature-time curve corresponding to initial velocity 1 m/s is also shown in figure 12. It is seen that ignition is more likely to occur for the impact fragment with small initial velocity.

4.4.4 Fuel/Air Mixture.

We have evaluated the thermal conditions that determine the likelihood of a fuel tank fire due to a hot fragment. In order for the fuel to ignite, it must not only be hot enough but there must also be a required mixture of fuel and air to permit combustion. This section presents an analysis of the fuel/air concentration near the fragment to determine if the mixture can ignite.

Consider a fragment that enters the liquid fuel section of the tank. After piercing the tank, the fragment will pull ambient air into the liquid fuel. The amount of air thus entrained will depend upon the frontal area of the fragment, the distance it travels into the tank prior to the liquid

readjoining at the point of penetration and the fragment velocity. For a cylindrical fragment, the volume of air, Vol_{air} , entrained is

$$Vol_{air} = xDL \quad (20)$$

where x is the integral of velocity with respect to time as given by equation 4.

The rate of vapor production is equal to the heat transferred due to boiling divided by the energy required for the phase change. The energy balance yields

$$h_{boil} \left(\frac{\pi DL}{2} \right) (T_S - T_\infty) = \dot{m}_{vap} [c_{v_v} (T_{sat} - T_\infty) + h_{fg}] \quad (21)$$

where T_S is the surface temperature of the fragment at the point of boiling. For an ideal mixture, the mole fraction of the vapor equals the volume fraction

$$\chi_v = \frac{m_{vap} / \hat{M}_v}{m_{vap} / \hat{M}_v + \rho_{air} Vol_{air} / \hat{M}_a} \quad (22)$$

where the mass of the vapor is given by equation 20, and the density of air is at atmospheric conditions.

At a particular distance, the liquid will close across the opening, and the air entrainment will cease. After this point, the fragment continues to vaporize the fuel, which causes the concentration to increase. Figure 13 illustrates the concentration of the vaporized fuel as a function of distance within the tank. For this calculation, a distance of three times the fragment diameter was chosen as the cavity length. This is justified for high Reynolds number flow. Fragments with two masses are studied. This process occurs very rapidly and the data in figure 13 are valid for times less than 1 msec. The fuel concentration is nearly constant while air is being entrained, because both the distance traveled and the vapor being produced are proportional to time. Over this time, all material properties, surface temperatures, and heat transfer coefficients are approximately constant, therefore the initial concentrations correlate with the initial conditions. The concentration of fuel during the entrainment process is a strong function of the initial velocity of the fragment. The Inconel fragment, having a higher initial temperature, produces a higher concentration due to the greater heat transfer by boiling. For even high initial temperatures and low initial velocity, the initial concentration is lower than the minimum 0.6% that is required for ignition (lower flammability limit).

Furthermore, it is possible that the entrained air will not maintain a single contiguous bubble. If the air breaks up into smaller bubbles, then the concentration of vapor in these bubbles will vary. The first bubbles will have a mixture of air and vaporized fuel at the initial conditions, which is below the lean flammability limit. Subsequent bubbles will grow richer in fuel vapor as the

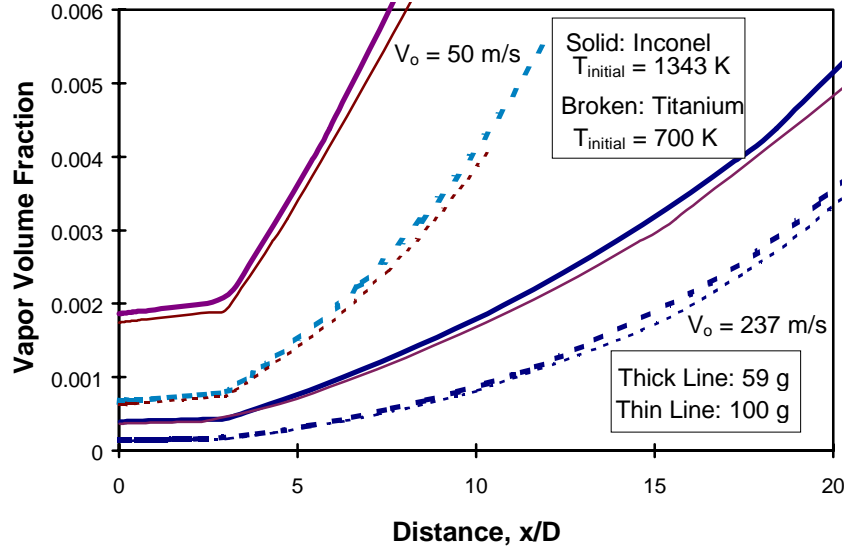


FIGURE 13. MASS FRACTIONS OF VAPOR IN THE WAKE OF A FRAGMENT IN LIQUID FUEL

air-laden bubbles rise from the moving fragment but because of convection their temperature will be too low for ignition to occur.

4.4.5 Bubble Rise.

As the fragment enters the tank, it entrains a certain amount of air from outside the tank in its wake. If the entry point is below the liquid level and ignition occurs as described in the previous section, the fire is limited to a bubble inside the liquid. This fire could extinguish quickly because of lack of air supply or rise to the liquid surface and ignite the vapor in the ullage. This section examines whether a bubble of hot vapor or an ignited fuel/air mixture formed in the liquid phase by a hot fragment can ignite the vapor in the ullage. Depending on the bubble number, size, and temperature, the hot vapor may or may not have enough energy to ignite the air/fuel mixture above the free surface of the liquid fuel. The bubble may exist long enough to ignite on its own, bringing very hot combustion products to the free surface of the fuel tank.

Fluid bubbles exist in a number of shapes from small spheres, or ellipsoids, to spherical-cap bubbles with a variety of wake formations. Clift et al. (1978) provide a method for determining the expected shape of a fluid bubble. The Bond and Morton numbers for a particular bubble determine its shape. Because the diameter fixes the velocity, the expected Reynolds number of the flow is determined by the Bond and Morton numbers.

$$Bo = \frac{g(\rho_l - \rho_v)D^2}{\sigma} \quad \text{and} \quad Mo = \frac{g\mu_l^4(\rho_l - \rho_v)}{\rho_l^2 \sigma^3} \quad (23)$$

We can model the vaporized fuel as an ideal gas:

$$P_v = \rho_v R T_v \quad \text{where } \rho_v = \frac{6m_e}{\pi D^3} \quad (24)$$

where D is the diameter of a volume-equivalent sphere, m_e is the mass of vapor inside the bubble, and P_v and T_v are the temperature and pressure of the vaporized fuel within the bubble. If the bubble forms at a distance, h_o , below the free surface, its pressure is

$$P_v = P_o + \rho_l g(h_o - Vt) + \frac{4\sigma}{D} \quad (25)$$

where V is the rise velocity of the bubble, σ is its surface tension, and ρ_l is the liquid density. We can neglect the surface tension of a bubble from 1 to 10 cm in diameter, because the pressure difference due to the surface tension will be less than 10 Pa. Examining this range for the volume-equivalent sphere and a flame temperature of 2000 K yields a range of Bond number from 25 to 2500. For kerosene, the Morton number is 1.6×10^{-9} . For this range of Bond and Morton numbers, the expected bubble shape is a spherical-cap bubble. The Reynolds number, based on the liquid properties and the diameter of the volume-equivalent sphere, should be between 10^3 and 10^4 (Clift et al., 1978). Such a bubble shape is depicted in the inset of figure 14.

The terminal velocity of a fluid bubble in liquids is related directly to their observed shape. Spherical-cap bubbles have a terminal velocity given by

$$V = 0.711 \sqrt{\frac{g(\rho_l - \rho_v)D}{\rho_l}} \quad (26)$$

for vapor bubble in liquid

We can now estimate the bubble velocity and diameter given its temperature and depth below the free surface by equations 24, 25, and 26.

As the bubble rises, it will lose energy to the cooler liquid fuel. An energy balance on the bubble yields

$$\frac{\overline{hA}}{m_b c_b} (T_\infty - T_v) = \frac{dT_v}{dt} \quad (27)$$

where c_b is the specific heat capacity for the gas within the bubble of mass m_b . In order to assess the temperature change as a function of time, we need to determine the average heat transfer coefficient \overline{hA} (in the units of W/K). For spherical-cap bubbles, which are broad and flat, the heat transfer is given by the following correlation (Clift et al., 1978):

$$\overline{hA} = 2.195 \sqrt{\rho_l c_l k_l} D^{3/4} \quad (28)$$

where D is the diameter of the volume-equivalent sphere, ρ_l is the density, c_l is the heat capacity, and k_l is the thermal conductivity of the liquid fuel, all in MKS units. Clift et al. (1978) give a mass transfer correlation of an analogous form. The derivation of this expression assumes that the heat transfer is independent of the vapor properties, meaning that the vapor within the bubble is well mixed. As a result, there is no temperature gradient within the bubble.

We can now determine the bubble diameter, velocity, rise distance, and temperature as a function of time by performing iterative calculations. Figure 14 shows the diameter of a spherical-cap bubble composed of 2 g of vapor for initial temperatures of 700 K and 1200 K. The choice of this mass of vapor is based on an initial bubble diameter of about 10 cm, which is on the order of the length of the fragment. The results indicate that the bubble diameter reduces quickly as it rises, indicating that we expect the bubble to cool. Also shown is the diameter of an air bubble starting at 2000 K to account for the situation where the vapor and air ignite to produce combustion products at high temperature.

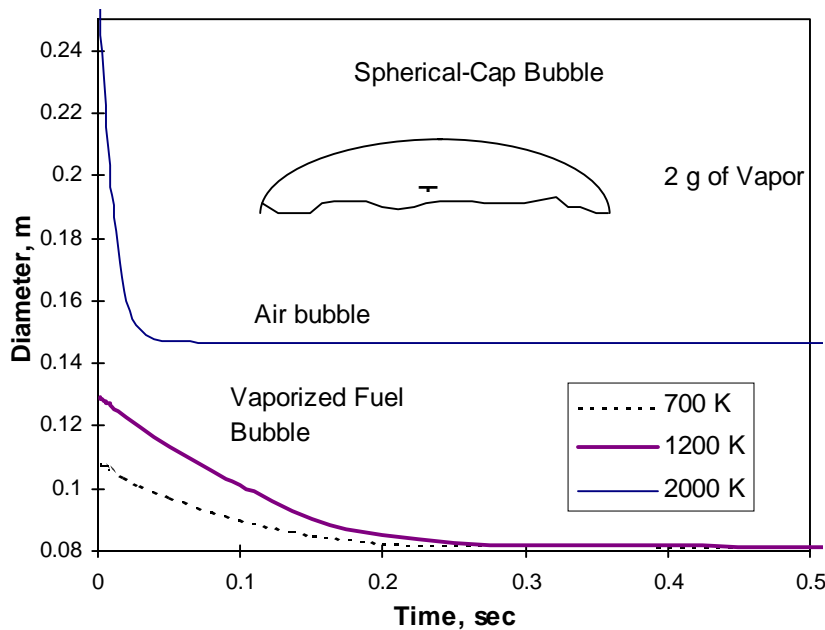


FIGURE 14. DIAMETER OF A BUBBLE RISING THROUGH LIQUID FUEL TO THE FREE SURFACE OF THE FUEL

An examination of the governing equations reveals that the only property of the bubble gas that enters the problem is the specific heat in equation 27. For a mixture of vaporized fuel and air, the specific heat will be smaller than that of pure fuel vapor; the time constant for the cooling will be decreased. We expect that a mixture of fuel and air will cool much more quickly, producing a rapid decrease in diameter as shown in figure 14. Even if the fuel ignites, producing products of combustion at 2000 K, the bubble will cool rapidly.

Figure 15 shows the results of the temperature calculation versus distance traveled by the bubble. Because the spherical-cap bubble has such a broad area and an active wake, the heat transfer

from the bubble is quite high. The temperature, therefore, rapidly decreases; the bubble rises only several centimeters before it cools considerably. This is equally likely for a bubble which has ignited prior to surfacing.

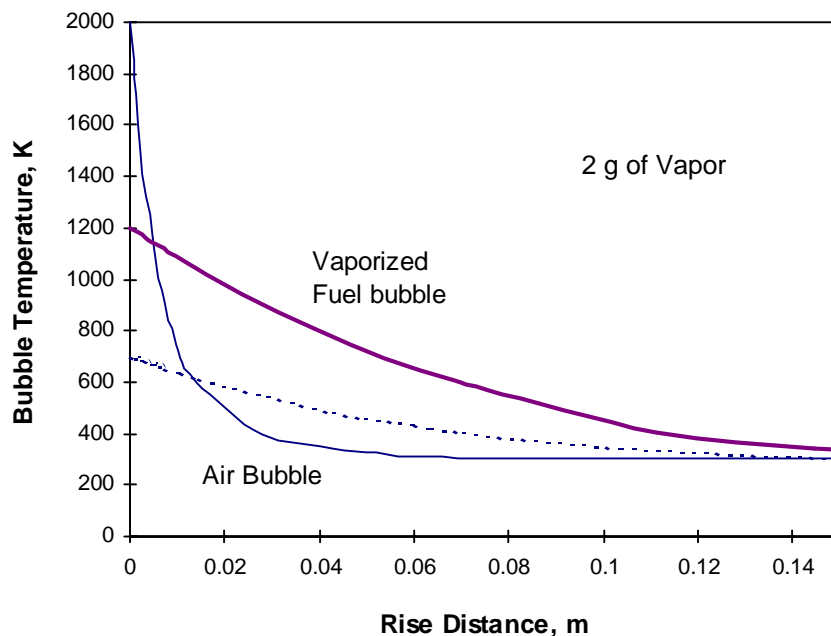


FIGURE 15. TEMPERATURE OF A BUBBLE RISING THROUGH LIQUID FUEL TO THE FREE SURFACE

The bubbles, therefore, can not be expected to produce ignition because of the rapid convection of energy to the liquid fuel. Only if the fragment travels very close to the free surface, do we expect favorable conditions for ignition. Under such a condition, there is a greater likelihood that the fragment would directly ignite the vapor above the free surface.

Even though ignition in the liquid phase may occur (as shown in the previous section), the effect of ignition in the bubbles is isolated to the liquid phase. The fire in these bubbles (if any) will go out without igniting the vapor in the ullage. Tank ignition, therefore, by impact within the liquid fuel can be neglected.

4.5 PASSAGE FROM LIQUID FUEL TO ULLAGE.

When a fragment enters the fuel tank in the liquid section of the tank, it will begin to cool rapidly. The velocity, however, is so high that the fragment may pass completely through the tank in the liquid phase (see figure 14). The fragment may also enter the ullage space after having traveled through the liquid (say on a diagonal path). The fragment may not have time to cool substantially before it enters the ullage space, because its velocity is so high, bringing it quickly into the vapor.

We have discussed the effect of agitation on the fuel/air mixture within the tank. The fragment itself may also create a mist as it leaves the liquid by pulling up the liquid with it.

This second mode of mist creation will add to the likelihood of a flammable fuel/air mixture. Considering our results of the temperature-time necessary for ignition, there is a high risk of fire or explosion of the fuel tank because of the additional mechanism for vapor production.

4.6 ANALYSIS LIMITATIONS.

The present analysis made a number of simplifications and assumptions in order to make the problems of the variation in fragment size and velocity tractable. For example, first, we simplified the fragment shape to a cylinder in cross-flow conditions. In fact, fragments are often multiple-blade sections and as such resemble plates with openings or gaps. We would expect that the larger area would expose more fluid to hot surfaces in the trailing area of the fragment. The extended wake and flat plate-like convection conditions could change our results.


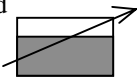
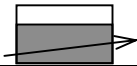
Second, we used an order of magnitude estimate for the wake size instead of calculating it based on considerations of wake dynamics, heat transfer, and combustion. These processes can alter the size, composition, and temperature within the wake and downstream of the fragment. Also, a larger wake may entail a temperature gradient across it, which we did not consider explicitly. Neglecting these effects is in keeping with our assumptions on fragment geometry and motion.

Third, we used the ignition delay time as a means to establish if the conditions for ignition are satisfied. The analysis can only determine if the conditions exist, but any investigation of the temperature or pressure after ignition has not been addressed. There are considerable avenues of investigation still to be examined, particularly when combinations of the aforementioned effects, such as flat fragment shapes, fragment tumbling, and reacting wakes occur. Only a more detailed analysis will permit any conclusions to be drawn under such conditions.

4.7 COMPARISON OF PRESENT STUDY WITH WALLIN.

As presented in section 3.4, Wallin (1976) evaluated an ignition risk factor for penetration of fuel tanks by hot engine debris. The conditions examined in his work (which were previously summarized in table 5) are now compared with our results in table 9. For the case of fragments that enter the ullage directly, Wallin assigned (based on judgment) an 80% probability of an explosion when the fuel temperature is within the flammability limits. For the case of fragments that pass through the liquid prior to entering the ullage, a 70% probability is assigned for a fuel temperature within flammability limits. These probability factors are consistent with our work in section 4 where we determined that the fuel/air mixture in the ullage and the temperature of the debris meet the criteria for ignition (summarized in table 9). Furthermore, we discussed that only a slight decrease in the likelihood of ignition would occur for fragments that enter the liquid prior to entering the ullage space. Wallin (1976) does not assess a probability for debris that enters the liquid fuel and does not reach the ullage. It is not clear whether Wallin did not consider this ignition mode or that he assigned it a negligible probability. In either case, it is consistent with our analysis, which showed that ignition is unlikely when the fragment enters the liquid phase and does not reach the ullage.

TABLE 9. COMPARISON OF IGNITION RISK FACTORS FROM WALLIN (1976) WITH PRESENT STUDY

	Will Ignition Occur?					
	Wallin (1976)			Present Study		
Fuel Conditions in Ullage Space	Mist Region ($T < T_{lean}$)		Temperature (T) Within Flammability Limits*	Mist Region ($T < T_{lean}$)		Temperature (T) Within Flammability Limits*
	Mist by Agitation	Mist by Fragment		Mist by Agitation	Mist by Fragment	
Penetration Scenario						
Fragment enters ullage above liquid 	not considered	N/A	80%	possible	N/A	Yes
Fragment enters ullage through liquid 	not considered	5% @ $T=-50\text{ }^{\circ}\text{C}$ rising linearly to 70% at T_{lean}	70%	possible	possible	Yes
Fragment enters only in liquid 	No			No		

*dependent upon the flight profile

The flammability limits, as defined in section 3, depend on both the flight profile and the fuel type and conditions. The flight profile determines the ambient temperature and pressure conditions. For Jet-A fuels, the static flammability limits lie outside the atmospheric conditions of interest. The mist region, however, becomes very important since it coincides with the pressure-temperature relation for standard and tropical atmospheric conditions. For the mist region, Wallin (1976) approximated the risk by assuming arbitrarily a 5% probability of ignition at -50°C , which rises linearly to 70% at the lean limit. He included this only for the case where the fragment first enters the liquid fuel. As a result, his assessment accounts only for the mist produced by the fragment as it passes out of the liquid, i.e., mist due to agitation, vibration, and sloshing is not taken into account.

As discussed in sections 3 and 4, the agitation effectively lowers the lean flammability limit by producing droplets which, when heated, effectively increase the concentration of the fuel/air mixture. For the mist region in table 9, we indicate only that ignition is possible since it depends on the complex issues which govern the degree of agitation or the manner in which the fragment travels through the liquid. The quality of the mist formed and its ease of vaporization by the hot fragment govern the possibility of ignition.

5. HYDRODYNAMIC RAM CALCULATIONS.

Projectiles (engine breakup debris) penetrating the fuel tank may generate intense pressure waves capable of rupturing the tank walls. This phenomenon, termed hydraulic ram, can lead to catastrophic loss of the aircraft. Massive fuel loss, resulting from fuel tank failure, can also lead to aircraft loss by onboard fires and by fuel starvation.

When a projectile travels through the fuel, the drag forces acting to decelerate the projectile are the source of pressure waves that propagate towards tank walls. Pressure loading incident upon a fuel tank wall may produce damage to the wall. The mechanism has been recognized in military but not commercial aircraft applications. Major work in this area has been carried out by the military over the last 25 years, culminating in various computer programs. This section applies a computer program available to us called ERAM (Lundstrom, 1988), to assess the potential damage if a fragment from either a fan blade or a turbine disk penetrates the fuel tank.

5.1 BRIEF DESCRIPTION OF ERAM.

The formulation of the analyses in ERAM can be summarized as follows:

- A force balance on the projectile determines the slow down of the projectile due to drag forces by the liquid. The analysis uses a constant drag coefficient that depends only on whether or not the projectile tumbles. This drag coefficient is determined by matching the model with test data.
- The kinetic energy lost by a projectile is computed and converted into total energy of the fluid (internal plus kinetic).
- Disturbances in the fluid are assumed to obey the linear acoustic wave equation. The pressure is then calculated by adding up the contributions of a series of spherical pressure waves centered along the projectile path.
- Before the fluid closes in on the hole, an elongated cavity is formed behind the fragment due to the entrainment of air (through the puncture in the tank) in the wake of the fragment.

The analyses in ERAM is based on a number of assumptions and approximations which may need improvement. While we do not agree with many of these assumptions, the code is the best available so far.

To apply ERAM, the inputs needed include: the shape, weight, impact velocity, orientation, and tumbling of the fragment; the geometry and size of the tank; and the density of the fuel.

5.2 DESCRIPTION OF TYPICAL FRAGMENT CHARACTERISTICS.

The detached fragments can be from a blade as well as from a disk. Table 10 shows the characteristics of various possible fragments of interest from fan, high pressure (HP) compressor, HP turbine, and low pressure (LP) turbine. The information on the HP turbine blades is identical to that used in the previous section.

TABLE 10. TYPICAL CHARACTERISTICS OF FRAGMENTS FROM
BLADES AND 120 DEGREE DISK SEGMENTS FOR COMMERCIAL
AIRCRAFT ENGINES

Component	RPM	Blade Mass (lbs)	Length (in)	Velocity (ft/s)	KE (ft-lbf)	Max Mass for Disk (lbs)	Radius (in)	Center (in)	Velocity (ft/s)	KE (ft-lbf)
Fan	5400	0.84	24	848	9390	25	6	3.31	156	3150
HP Compressor	7200	0.10	4.5	833	940	80	11	6.06	381	60200
HP Turbine	7200	0.13	6.7	776	1220	70	9	4.96	312	35300
LP Turbine	5400	0.22	11	872	2520	172	13	7.17	338	102000

Since the information on any particular aircraft is proprietary and we are interested in generic information, table 10 was compiled based on data from various sources including Mattingly (1987) and aircraft specification and designs in the open literature.

The second column in table 10 is the rotation speed of the blades and disks in revolutions per minute. The mass, length, velocity, and translational kinetic energy of a blade are provided. The size of the disk fragment is assumed to be one-third of the whole disk. Typical mass, radius, center of mass, velocity, and kinetic energy of the 120 degree disk are also presented.

Since the fragment with the largest kinetic energy causes maximum damage to the fuel tank, we selected the fan blade and LP turbine disk sector for the calculations. We model the fragment as a long cylinder, a thin cylinder, and as a sphere, which are the geometrical shapes accepted by the ERAM program. We calculate below the volume-equivalent dimensions for these three shapes. They are denoted as Models B1, B2, and B3 for the blade and D1, D2, and D3 for the disk.

5.2.1 Blade Fragment Models.

We assume the material of the fan blade is titanium. For a commercial aircraft fan blade, the volume is

$$\text{Volume} = \frac{0.84 \text{ lb}}{0.1685 \text{ lb / in}^3} = 5 \text{ in}^3$$

For Model B1 (long cylinder), the blade fragment impacts the fuel tank with the smallest contact area:

$$L = 24 \text{ in}$$

$$D = \sqrt{\frac{4}{\pi} \times \frac{5 \text{ in}^3}{24 \text{ in}}} = 0.52 \text{ in}$$

For Model B2 (thin cylinder), the fragment impacts the fuel tank with largest contact area. The width of the blade is assumed to be 1.2 in.

$$D = \sqrt{\frac{4}{\pi} \times 1.2 \text{ in} \times 24 \text{ in}} = 6.1 \text{ in}$$

$$L = \frac{5 \text{ in}^3}{1.2 \text{ in} \times 24 \text{ in}} = 0.174 \text{ in}$$

For Model B3 (sphere), the fragment is modeled as a sphere.

$$D = 2 \sqrt[3]{\frac{3 \times 5 \text{ in}^3}{4\pi}} = 2.12 \text{ in}$$

5.2.2 Disk Sector Fragment Models.

We assume the LP turbine disk material is Rene 80; many other commonly used disk materials have similar properties. The volume of the 120 degree sector is

$$\text{Volume} = \frac{120}{360} \times \frac{172 \text{ lbs}}{0.2960 \text{ lb/in}^3} = 194 \text{ in}^3$$

For Model D1 (long cylinder), small impact area

$$L = 13 \sqrt{3} \text{ in} = 22.5 \text{ in}$$

$$D = \sqrt{\frac{4}{\pi} \times \frac{194 \text{ in}^3}{22.5 \text{ in}}} = 3.31 \text{ in}$$

For Model D2 (thin cylinder), large impact area

$$D = \sqrt{\frac{4}{\pi} \times \frac{120}{360} \times \pi \times 13^2} = 15 \text{ in}$$

$$L = \frac{4 V}{\pi D^2} = 1.1 \text{ in}$$

For Model D3 (sphere), the fragment is modeled as a sphere

$$D = 2 \sqrt[3]{\frac{3 \times 195 \text{ in}^3}{4 \pi}} = 7.18 \text{ in}$$

5.3 DESCRIPTION OF A TYPICAL FUEL CELL.

There are several cells in an aircraft fuel tank. We choose the one with the following dimensions in our calculation:

80 in x 21.5 in x 17 in

which corresponds to a segment of a Boeing 737 wing between two stiffeners.

5.4 ERAM DATA INPUT.

The following assumptions are used in running the ERAM code:

- a. No reflection of pressure waves from the tank walls.
- b. Fragment penetrates from the center of the bottom wall of the fuel tank to the center of the top wall. The fragment does not tumble in the fuel tank.
- c. The fuel density is the same as kerosene, 0.02962 lb/in^3 , sound speed = 4330 ft/sec.
- d. The tank wall is made of 0.06-in.-thick aluminum. There is no foam attached to the tank wall. The critical stress intensity factor at room temperature for aluminum alloy 7075-T6 is $K_{IC} = 28.6 \text{ MN m}^{1/2}/\text{m}^2 = 26 \text{ ksi in}^{1/2}$, from Avallone and Baumeister (1986).
- e. The blade and the disk are made of titanium and Rene 80 respectively.
- f. Ambient pressure is 12.24 psi, for an aircraft at 1500 m altitude.
- g. Failure criteria is when the plate stress, σ_p , exceeds the maximum allowed stress, σ_{\max} , before the fracture.

$$\sigma_p = \frac{K_{IC}}{\sqrt{Q\pi d_I}} > \sigma_{\max} = \frac{K_{IC}}{\sqrt{Q\pi d_{cr}}}$$

where K_{IC} is the critical stress intensity factor Q is a geometric factor that includes the effect of wall thickness, σ_{\max} is the maximum stress the plate can endure, d_I is the initial hole size on the entry plate after the penetration of the projectile, and d_{cr} is the critical initial hole size (flaw diameter in ERAM). Thus, the wall fails when $d_I > d_{cr}$.

5.5 RESULTS OF CALCULATION.

Three cases of each model, as described above, are investigated in modeling the hydrodynamic ram effect of both blade and disk. Figure 16 shows the peak pressure distribution acting on the entry wall as a function of time. The wall pressure is the summation of the dynamic pressure and the static pressure acting on the entry wall. As the fragment travels through the fuel tank, its

velocity drops, depending on the mass and cross-flow sectional area of the fragment. A fast projectile velocity drop corresponds to a larger pressure pulse amplitude.

The peak stress history of the wall is shown in figure 17. A larger wall pressure pulse results in a large wall stress and consequently a large strain. The critical initial hole size (d_{cr}) is shown in figure 18. We assume that the initial hole size (d_i) is the width of the perforation hole produced by impact: 1.2 in. for the blade and 13 in. for the disk radius, both plotted as horizontal lines in figure 18. If the initial hole size exceeds the critical hole size ($d_i > d_{cr}$), the wall further fractures and fails. This failure criterion is well satisfied for all cases, except for model B1 where it is only marginally satisfied. Model B1 is the least severe case since the blade impacts the fuel tank with the smallest contact area.

In summary, for the conditions investigated in this study, the ERAM calculations show that a fuel tank can fail if it is impacted by fragments such as a blade or disk segment. The occurrence of failure depends on a number of parameters including fragment size, shape, velocity, and impact angle. Thus, the hydrodynamic ram hazard should not be discounted.

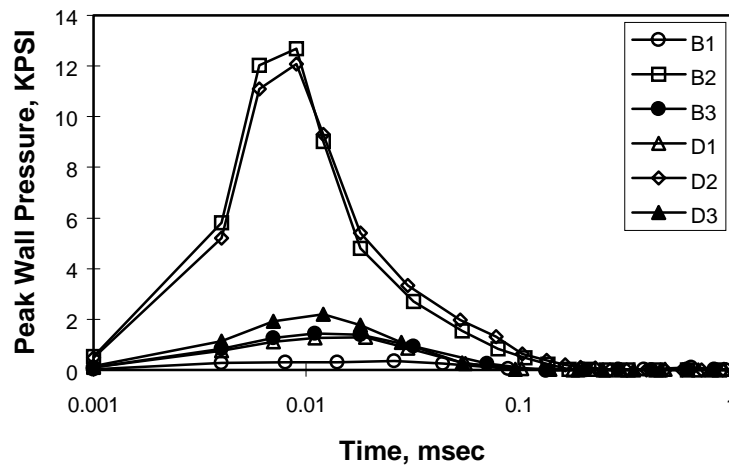


FIGURE 16. PEAK WALL PRESSURE EVOLUTION AFTER FRAGMENT IMPACTS THE FUEL TANK

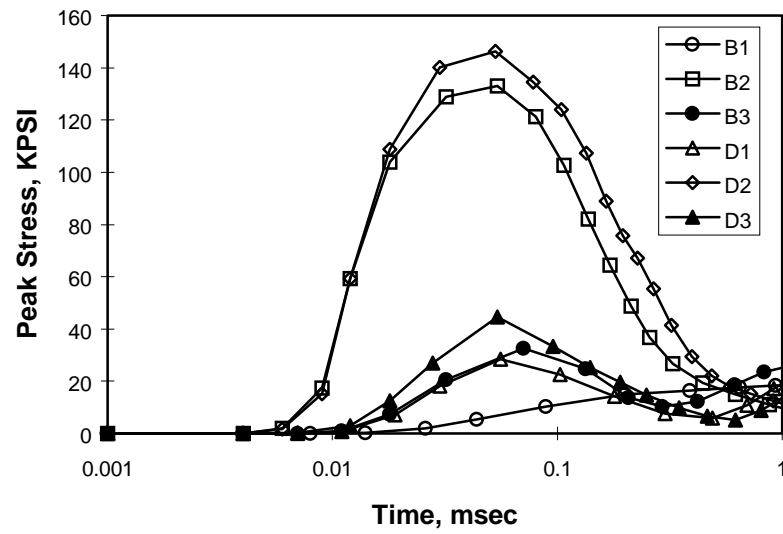


FIGURE 17. PEAK STRESS IN THE TANK WALL AS A FUNCTION OF TIME

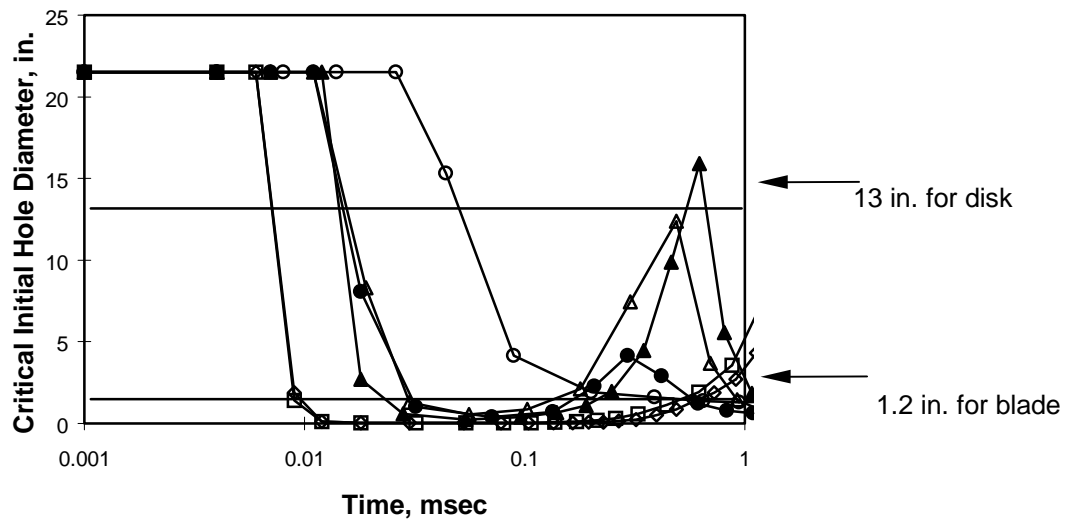


FIGURE 18. CRITICAL INITIAL HOLE DIAMETER ON THE WALL (MAXIMUM ALLOWABLE INITIAL HOLE SIZE AS A FUNCTION OF TIME). THE TWO HORIZONTAL LINES REPRESENT THE INITIAL HOLE SIZE DUE TO THE PERFORATION OF BLADE AND DISK FRAGMENTS.

6. POSSIBLE MITIGATION MEASURES.

Shielding and containment of engine fragments has received significant attention over the years. If such protection fails and tank penetration occurs, it is still possible to protect against a fuel tank fire and hydrodynamic ram. This section presents a qualitative discussion of the types of protection measures that might be considered. The adoption of any preventive measure depends on detailed cost-benefit analyses which are beyond the scope of this report.

6.1 MITIGATION OF FIRE AND EXPLOSION.

Protection of fuel tanks in military aircraft is provided by making the vapor in the ullage space inert and by using foams and extinguishing agents. These systems are described briefly below for reference only. We make no judgment on the cost/benefit of any of these systems to commercial aircraft.

6.1.1 Ullage Inerting.

The vapor in the ullage space can be made inert by limiting the oxygen to levels that will not support combustion. Stewart and Starkman (1955) determined that sustained combustion cannot occur within the fuel tanks if the volumetric oxygen concentration is 9 percent or less. This concentration is obtained by injecting nitrogen from a source external to the fuel tank. Such sources include

- Storage bottles of liquid nitrogen (LN_2 dewars) as used on the Air Force C-5 fleet. This system has the disadvantage of requiring a supply of cryogenic nitrogen nearly every time the airplane is refueled—an unacceptable logistics problem in today's airports. We understand that the current C-5 fleet leaves its LN_2 system uncharged!
- Onboard inert gas generator systems (OBIGGS). Such a system is placed onboard the F-18, C-17, and F-22 aircraft. It processes engine bleed air into a nitrogen-rich (inert) gas. The OBIGGS eliminates the logistics problems of liquid nitrogen resupply and produces oxygen as a by-product, which can be used on the aircraft. It, therefore, is preferred over the liquid nitrogen system.

A basic limitation of both systems is the release of fuel-dissolved oxygen. In an airport fuel storage tank, the fuel contains significant amounts of dissolved air (oxygen and nitrogen) in thermodynamic equilibrium at ambient pressure. The air-saturated fuel is loaded onto the plane. Upon airplane climb, natural evolution of dissolved oxygen could quickly cause an initially inert ullage to become flammable.

The dissolved oxygen can be scrubbed out by bubbling an inert gas through the fuel. The high contact area between the gases in the bubbles and the dissolved oxygen in the fuel tend to cause the composition of the gases in the bubbles to equilibrate with dissolved gases in the fuel. Dissolved oxygen outgasses more readily than dissolved nitrogen. Thus, the bubbles remove oxygen from the fuel and transport them into the ullage from which they can be expelled through the fuel tank vent system.

All of the above systems contribute to weight, volume, and auxiliary power requirements. Furthermore, the complexity of these measures and their associated impact on reliability and maintenance increase both initial and operating costs.

6.1.2 Foams.

Stewart and Starkman (1955) showed that foam, placed within a fuel tank, suppresses ignition and damage due to overpressure. The foam used was a 30 kg/m³ open cell, polyurethane foam, filling 65 percent of the tank. The limited stability of this foam (at fuel temperatures of 80°C and in the presence of water) poses a continual danger of disintegration and potential blockage of filters, coolers, sensor lines, etc. by pieces of the foam. Also, the limited life of the foam (only some hundred flying hours) required several changes during the life of the aircraft, increasing maintenance costs. Foam systems have been installed on the C-130, A-10, and the F-15.

Modern foams do not suffer from stability problems. For example, polyamide foams (networks) are stable for an unlimited period at temperatures of 100°C, with short excursions up to 130°C. Tests have shown that an 80 percent foam fill (with a density of 8.5 kg/m³) leads to acceptable overpressures during an in-tank explosion (Wördehoff, 1989).

Thus, foams can provide effective explosion protection for the fuel tanks, and have the added advantage of being a passive system (no moving parts). However, they contribute to weight and volume penalties, suffer from the potential for premature disintegration, are prone to electrostatic problems, and increase maintenance costs.

6.1.3 Extinguishing Agents.

Active systems have been developed to inject extinguishing agents into the ullage when a hazardous condition is detected using fast optical detectors. The most common and effective agent is halon. It is used on the F-16, but, it has been banned from production because of its adverse impact on the ozone layer. The conflicting issues of performance, practicality, and cost, posed by potential replacements of halon, are a subject of extensive research and development (R&D) which has yet to be resolved.

6.2 MITIGATION OF HYDRODYNAMIC RAM.

There is one commercially available technology for hydrodynamic ram mitigation in military aircraft. It consists of foam backed structural panels and is used on military helicopters (CH-47 and UH-60). Hydrodynamic ram is attenuated by foam compression although the protection is generally not enough. This technology is in a great state of flux as new foams are being tried. Each foam has advantages and disadvantages.

Also, hydrodynamic ram mitigation is a subject of significant R&D. Various technologies are being tried, one of the most advanced of which is a Nitrogen-Inerted Bladder by Boeing (NIBB). In this system, porous bladders are placed on each of the tank walls. Nitrogen is pumped into the bladders, inflating them, then oozes out through the pores of the bladders and fills the ullage, inerting it. According to Boeing the system provides protection against both

- hydrodynamic ram since the bladder cushions the shock impact near the wall and
- fire/explosion since the nitrogen inerts the ullage.

However, the system has limitations. At the edge of each wall where the bladder is attached, inflation is necessarily zero. Thus there is no protection at the corners where two edges meet. Also, nitrogen gas is needed as an expendable.

Note that before full commercial development of any such system from military applications, its suitability would have to be demonstrated. A cost benefit analysis is also required.

7. SUMMARY AND CONCLUSIONS.

7.1 SUMMARY.

The report presents an exploratory assessment of the potential for in-tank fire and hydrodynamic ram caused by uncontained engine failures. The effort covers a review of accident data and of pertinent literature, the development of analysis specifically for this project, and the use of an existing computer code.

The two accident scenarios of interest cover a sequence of events; namely, uncontained engine failure, penetration of the fuel tank by engine debris, ignition of the fuel inside the tank or hydrodynamic ram (pressure rise inside the tank), and tank rupture. Section 2 presents a preliminary review of historical accidents involving uncontained engine failures. The purpose was to characterize the sequence of events that may lead to catastrophic loss of the aircraft triggered by uncontained engine debris. While the above sequence of events has not been reported in any particular accident, some of these events have been reported singly or in various combinations.

For example, there are many reports of historical accidents involving fragments from an uncontained engine failure penetrating fuel tanks with significant damage to the tanks. Occasionally, there are reports on fuel tank ruptures and the outpouring of fuel from the tank, as well as fuel tank fires and explosions. Fuel tank ruptures clearly indicate that pressure forces were developed inside the fuel tank – although it is not known whether they are due to combustion or hydrodynamic ram effects. In a few cases, ignition and fire inside the tank are reported, while no report of hydrodynamic ram has been found. Despite the lack of evidence for the aforementioned sequence of events occurring in their entirety, taken separately, the events of interest appear to happen and pose a threat to the fuel tanks. Clearly, a definitive resolution of this issue cannot be achieved from our quick review of accident data. However, even the fragmented evidence found suggests the need for further study of the scenarios under consideration. In appendix A, we present a summary of these pertinent accidents.

Our review also identified that damage to the fuel tank can produce fuel leakage resulting in other adverse impacts to the aircraft. For example, fuel can leak into dry bays and engine nacelles, be ingested by an engine, or pool onto the ground (for a stationary aircraft). The fires resulting from such leakage can pose great danger to an aircraft structure. These scenarios have

occurred in the past (such as the Manchester accident in 1985) and may be more important than those examined in this study. They should be considered in future work.

Since historical evidence was fragmented and limited, we gave particular attention in this project to what might happen based on considerations of the fundamental processes involved in fuel tank ignition and hydrodynamic ram.

7.1.1 In-Tank Fuel Ignition by Engine Debris.

The first question was to determine whether the fuel tank contains a flammable mixture under the conditions of this study. Section 3 presents pertinent information from the literature on the flammability of the ullage of an aircraft fuel tank containing Jet-A fuel. It is well known that the fuel vapor/air concentration inside a vented aircraft tank at typical ambient temperatures is not flammable at sea level nor at altitude. In other words, the ullage is outside the static (or equilibrium) flammability envelope. However, it is also well documented in the literature that dynamic processes can broaden significantly the flammability envelope over the static case. The most important of these processes is the formation of a mist of fuel droplets inside the tank due to fuel sloshing under normal aircraft vibration and motion. When such droplets are vaporized by a hot fragment, they effectively raise the fuel vapor pressure in the ullage making it flammable.

A fuel mist can also be produced by the motion of a fragment through the fuel. This is supported by test data on JP-5 and -8—two military fuels that are comparable in volatility to Jet-A fuel. The tests involve gun fire impact against a “static” tank with the projectile entering below the liquid level and exiting into the ullage. Ignition occurred at fuel temperatures well below their flash points and was interpreted by the test engineer as resulting from a mist produced by the projectile motion.

In this project, both mechanisms of spray formation, due to motion of aircraft and fragment, are of interest. They enrich the vapor concentration in the ullage and broaden the flammability envelope thus increasing the likelihood of ignition inside the tank.

The risk of fire and explosion in aircraft fuel tanks in the Concorde SST due to uncontained failure of the Olympus 593 engine was studied by British Aerospace (Wallin, 1976). For the case of fragments entering a flammable ullage directly, Wallin assigned, based on judgment, an 80 percent probability of fire. For the case of fragments that pass through the liquid prior to entering the ullage, he assigned a probability that increased linearly with fuel temperature from 5 percent at -50°C (well below the flash point) to 70 percent at the temperature corresponding to the lean limit. These probability values are consistent qualitatively with our work in section 4, where we determined that ignition can occur since the fuel/air mixture in the ullage, the temperature of the debris, and the fragment transit time meet ignition criteria taken from the literature.

In summary, our literature review in section 3 indicates that the ullage inside a fuel tank with Jet-A can be flammable under operating conditions. Because the ignition potency of projectiles in military tests is very different from that of debris from an uncontained engine failure, the next

question becomes whether the debris provides enough of a heat source to ignite the fuel. This question is addressed in section 4.

We focus on debris originating from the high-pressure turbine because they have the highest initial temperature, and consequently, the greatest potential for ignition. While impacting a fuel tank, the temperature of the debris may change due to secondary effects such as heat produced by friction (as illustrated in appendix B) or heat transferred to intervening structures. Such effects are very difficult to quantify, and are thus not examined in this study.

We focus on the occurrence of ignition and its dependence on fragment size, temperature, and velocity, as well as fuel properties. By examining the effect of heat transfer and vapor formation in the fragment wake, we determined whether a hot fragment can ignite the fuel before it cools down significantly.

Section 4 investigates two scenarios: first, a fragment enters the tank and travels through the ullage. Consideration of convective heat transfer from the fragment to the ullage gases permits us to determine the temperatures of the fragment and its surrounding vapor film as a function of time. We compare the temperature-time history of this film with that required for fuel ignition as measured in fundamental studies (Spadaccini and TeVelde, 1982). This comparison delineates regimes of ignition and no ignition. The latter occurs because either the fragment is not hot enough or it exits the tank too quickly.

The second scenario involves the heating of the fuel as the hot fragment enters and travels through the liquid portion of the tank. An analysis similar to that of the ullage is carried out with the addition of boiling and radiative heat transfer from the fragment. We also consider the motion of the vaporized fuel as a bubble that rises to the free surface of the fuel tank, where it may ignite the vapor in the ullage. Ignition may take place within the bubble as it rises or when it hits the free surface depending on the rate of heat transfer.

The heat transfer analysis indicates whether the temperature-time history of the film supports ignition conditions. In addition, the fuel/air mixture must be in the flammable range for the fuel to ignite. We estimate in a preliminary way the concentration of fuel in the wake of the fragment in order to refine our assessment of the likelihood of ignition. For the case of the ullage, we approximate the increase in the concentration of fuel in the mist region. For the liquid case, we calculate the amount of fuel vaporized and consider the amount of air entrained within the fragment's wake.

The foregoing analyses provide a simplified evaluation of the conditions under which a fuel tank fire may ignite by hot engine parts from a catastrophic failure of a turbine. For a fragment that enters the ullage, both the composition of the fuel/air mixture and the temperatures are sufficient to ignite a fire within the fuel tank in the presence of mechanical agitation (either by aircraft or fragment motion).

For a fragment traveling through the liquid fuel, we found that while there exists a sufficient fragment temperature to promote ignition, the fuel/air concentrations necessary for ignition do not exist, even with air entrainment in the wake of the fragment. Thus, ignition is not likely.

Even if it were to occur in a bubble inside the liquid, it will not persist due to significant quenching as the bubble rises through the liquid fuel. We expect any ignition within the liquid to be contained within the liquid phase. Tank ignition, therefore, by impact within the liquid is unlikely.

For fragments that enter the liquid phase and cross into the ullage space, ignition of the vapor depends on the temperature of the fragment as it makes the transition. Our results indicate that because the velocities of the fragments are so high, a fragment still within the tank that crosses to the ullage will have a sufficient temperature to ignite the vapor. On the other hand, a fragment that enters the tank in the ullage space will quench upon entering the liquid fuel.

Upon ignition, explosive pressures may or may not be produced, depending on the amount of the fuel/air ready for immediate combustion upon ignition as well as the penetration hole size produced by the fragment. As such, many of the issues addressed in the analysis of ignition (fuel temperature, altitude, mist formation, etc.) are also important to the analysis of explosion. Also, the effect of hole size would have to be accounted for in the analysis—the larger the hole the smaller the pressure rise. In view of the uncertainties involved in quantifying these issues, focusing on ignition (the primary event) seemed more reasonable than explosion (a secondary event). Also, one can conservatively assume that upon ignition, the fuel tank is at-risk because combustion pressures are much higher than the design pressure of the tank. Calculating the overpressure, given ignition, can be done using the type of analyses presented in this report.

7.1.2 Hydrodynamic Ram by Engine Debris.

When a fragment penetrates a tank, it slows down as it travels through the fuel due to liquid drag forces. Part of the fragment kinetic energy is converted into fluid mechanical energy – an effect called hydrodynamic ram. The ram pressure loads the tank walls and forces them to bulge and tear, greatly increasing the size of the puncture hole produced by the fragment. A large amount of fuel can then flow out of the tank and find its way to an ignition source (such as a hot surface or torn electrical wires). Loss of fuel can also lead to loss of center of gravity control and potential loss of the aircraft.

This mechanism has been recognized in military but not in commercial aircraft applications. Major work in this area was carried out by Eric Lundstrom (1988), culminating in a computer program called ERAM. This code was developed for the case of a projectile impacting a fuel tank. The code uses inputs describing a projectile (shape, weight, impact velocity, orientation, and tumbling), fluid properties (density and speed of sound) and a rectangular tank (size and panel materials) to compute pressure as a function of time at various coordinate locations. The formulation of ERAM is based on a number of assumptions and approximations with which we do not agree and which may need improvements. Still, the code was available to us, and the predicted trends were plausible.

Section 5 presents the results of parametric calculations with this code for the case of a typical fan blade and a low-pressure turbine disk segment (engine break-up fragments with the largest kinetic energy). The results of ERAM indicate that the tank can fail. Thus, the hydrodynamic ram hazard should not be ignored.

Protection methods against hydrodynamic ram are limited and still under development by the military. Protection methods against in-tank fire and explosion have been developed and used by the military for over two decades. These systems will incur weight, volume, or auxiliary power penalties, and require the addition of complex systems with their own reliability and maintenance issues (as briefly reviewed in section 6). Studies are needed to optimize these systems to particular applications and to trade off their cost and impact on airplane performance with safety improvement. In addition, detailed cost benefit analyses are required to determine whether such systems are desirable in commercial aircraft fuel tanks.

7.2 CONCLUSIONS.

Based on our review of literature data and on a theoretical study of heat transfer from a hot fragment to the fuel, we have determined that under the conditions of this study:

- Ignition is possible for a fragment impacting the ullage, even though the fuel is below the flash point. The presence of fuel droplets in the ullage and their heating and evaporation by the hot fragment raises the vapor pressure of the fuel locally. Ignition requires high temperature blade materials such as Inconel.
- Ignition is improbable for a fragment traveling through the liquid fuel.

By applying an existing computer code on hydrodynamic ram to typical fuel tank fragment impact conditions, we have determined that fragments with the highest kinetic energy (such as a typical fan blade or an LP turbine 120 degree disk segment) can fail the tank wall by the ram effect.

Thus, while there have been no historical accidents involving fire or hydrodynamic ram inside fuel tanks initiated directly by uncontained engine debris, our technical analyses of these events indicate that they can happen. Our extrapolation of limited accident data suggests that their probability is very low (less than 7×10^{-10} event/engine hour). Nevertheless, in-tank fires have occurred during uncontained engine failure, producing catastrophic aircraft losses, although not directly due to fragment impact. The possibility of these and other fire and explosion scenarios should be examined in future work using the approach presented in this report.

8. REFERENCES.

- Avallone, E.A. and Baumeister T. III (1986) Marks' Standard Handbook for Mechanical Engineers, Ninth Edition, McGraw-Hill Book Company.
- Botteri, B.P., et al., "A Review and Analysis of the Safety of Jet Fuel," AFAPL-TR-66-9.
- Clift, R., Grace, J.R., and Weber, M.E., 1978, *Bubble, Drops, and Particles*, Academic Press, New York, Chapter 2, pp. 26-27, Chapter 8, pp. 203-207, 213-216.
- CRC Report No. 530, 1983, "Handbook of Aviation Fuel Properties," Society of Automotive Engineers.
- FAA/SAE Committee on Uncontained Turbine Engine Rotor Events, *Aerospace Information Report*, No. 4770, July 1994.
- Frankenberger, C., "Uncontained Engine Debris Damage Mitigation Program," Naval Air Warfare Center, presented at the Second Workshop on Uncontained Engine Debris Characterization, Modeling and Mitigation, January 23-24, 1996, in Livermore, CA.
- Incropera, F.P. and DeWitt, D.P., 1985, *Fundamentals of Heat and Mass Transfer*, Wiley & Sons Inc., New York, Chapter 7, pp. 333, 336, Chapter 10, p. 469, Appendix A, pp. 757-758.
- Johnson, A.M., Roth, A.J., and Moussa, N.A., 1988, "Hot Surface Ignition Tests of Aircraft Fluids," Technical Report AFWAL-TR-88-2101, Wright-Patterson AFB, November.
- Kosvic, T.C., et al., 1971, "Analysis of Aircraft Fuel Tank Fire and Explosion Hazards," AFAPL-TR-71-7, March.
- Lundstrom E. (1988) "Structural Response of Flat Panels to Hydraulic Ram Pressure Loading," NWC TP 6770.
- Manheim, J.R., 1973, AFWAL-TR-73-76, Wright-Patterson AFB.
- Mattingly, J.D., Heisler, W.H., and Daley, D.H., 1987, *Aircraft Engine Design*, American Institute of Aeronautics and Astronautics, Washington, D.C., pp. 566-567.
- Maxwell, J.B., 1950, *Databook on Hydrocarbons*, D. Van Nostrand Co. Inc., New York, pp. 42, 91, 174, and 215.
- Moussa, N.A., 1980, "Aerodynamic Analysis of Aircraft Fires," Technical Report AFWAL-TR-80-3079, Wright-Patterson AFB, August.
- Moussa, N.A., 1990, "Flammability of Aircraft Fuels," SAE Technical Paper Series 901949, Aerospace Technology Conference & Exposition, Long Beach, CA, October 1-4.
- Mullins, B.P., 1953, "Studies on the Spontaneous Ignition of Fuels Injected into a Hot Airstream," Parts I-III, *Fuel*, Vol. 32, pp. 211-252, 327-342.

- National Transportation Safety Board, *Special Study: Turbine Engine Rotor Disk Failure*, NTSB-AAS-74-4, December 1974.
- Nestor, L., 1967, "Investigation of Turbine Fuel Flammability Within Aircraft Fuel Tanks," Report No. DS-67-7 prepared by Naval Air Propulsion Test Center for the Federal Aviation Administration, Washington, D.C.
- Pedriani, C.M., 1970, "A Study of the Fuel/Air Vapor Characteristics in the Ullage of Aircraft Fuel Tank," U.S. Army Aviation Materials Lab, AD 873252, June.
- Perry, J.H., 1950, *Chemical Engineer's Handbook*, 3rd Edition, McGraw-Hill, New York, pp. 459, 565, and 604.
- SAE Committee on Engine Containment, "Report on Aircraft Engine Containment," SAE AIR 1537, October 1977.
- SAE Committee on Engine Containment, "Report on Aircraft Engine Containment," SAE AIR 4003, September 1987.
- Spadaccini, L.J. and TeVelde, J.A., 1982, "Autoignition Characteristics of Aircraft-Type Fuels," *Combustion and Flame*, Vol. 46, pp. 283-300.
- Spadaccini, L.J., 1977, "Autoignition Characteristics of Hydrocarbon Fuels at Elevated Temperatures and Pressures," *Journal of Engineering for Power*, January, pp. 83-87.
- Stewart, P.B. and Starkman, E.S., 1955, "Inerting Conditions for Aircraft Fuel Tanks," WADC Technical Report No. 55-418, September.
- Wallin, J.C., 1976, "Engine Non-Containment-Risk Assessment Methods," British Aerospace Aircraft Group, Weybridge-Bristol Division, Britain.
- Wördehoff, J., 1989, "On-Board Fire and Explosion Suppression for Fighter Aircraft," AGARD-CP 467, Aircraft Fire Safety, NATO Advisory Group for Aerospace Research and Development, May.

APPENDIX A—DESCRIPTION OF KEY ACCIDENTS

A.1 NOTE ON DATABASES.

Data from previous accidents involving uncontained engine failures were compiled from many different sources including the National Transportation Safety Board (NTSB) accident reports and special reports, computerized databases, and Society of Automotive Engineers (SAE) reports. Another source of individual aircraft accident reports is the Air Accidents Investigation Branch from the British Department of Transport, who produced detailed accident reports similar to the NTSB. We also conducted a brief search of the computerized Federal Aviation Administration (FAA) Aircraft Accident Incident databases.

The NTSB database covers the years 1962 to present containing all the information on the accident report from NTSB 6120.4 or its predecessor. The files contain additional information not published in the cause report. The FAA Accident/Incident Database covers general aviation accident reports from 1973, general aviation and air carrier accident reports from 1978, and air carrier accident reports from 1982. Another database, the FAA Service Difficulty Report, was identified but not used. It covers general aviation and air carrier aircraft from 1974. The sources for this database include the Malfunction or Defect Report for general aviation and the Mechanical Reliability Reports for air carriers.

Specific reports on uncontained engine failures provide the most concise information on the causes of such failures and is invaluable in producing the fault tree analyses presented in section 2. However, these reports do not address the development of events after failures, leading to catastrophic loss of the aircraft. They include the “Report on Aircraft Engine Containment” from the Society of Automotive Engineers (SAE) Reports AIR 1537, AIR 4003, and AIR 4770, which cover three study periods: 1962 to 1975, 1976 to 1983, and 1984 to 1989, respectively. In addition, the NTSB published a report titled, “A NTSB Special Study of Disk Failures from 1962 to 1973,” which presents data on 41 cases of engine disk failures in public transport aircraft.

A.2 DESCRIPTION OF KEY ACCIDENTS.

This appendix summarizes five accidents relevant to this project. The first four present cases of uncontained engine failure with fuel tank punctures and/or fires. The Manchester, UK, accident briefly discussed in section 2 is presented in more detail here. This is one of the two cases where the fuel vapor in the ullage ignited and resulted in an explosion inside the fuel tank.

The last accident summarized is the uncontained engine failure of a DC-10 at Sioux City, Iowa, where all hydraulic systems were damaged and the aircraft was left with no flight control. Although no fuel systems were directly affected by this engine failure, we included this accident to further demonstrate the destructive consequences of an engine failure. The ability of engine fragments to exit the engine casing and still have enough energy to penetrate external and internal aircraft structure suggests their ability to also penetrate aircraft fuel tanks.

A.2.1 Manchester, UK, August 22, 1985.

About 36 seconds after takeoff roll, as the aircraft speed passed 125 knots, the left engine of a Boeing 737-2367 series 1 suffered an uncontained failure, which punctured an access panel on a fuel tank. Fuel leaking from the wing ignited and burned as a large plume of fire trailing directly behind the engine. The crew mistook the sound of the engine failure for a tire failure or bird strike and abandoned the takeoff immediately, intending to clear the runway. They had no indication of fire until 9 seconds later, when the left engine fire warning occurred. After an exchange with Air Traffic Control, during which the fire was confirmed, the commander warned his crew of an evacuation from the right side of the aircraft, by making a broadcast over the cabin address system, and brought the aircraft to a halt.

As the aircraft turned off the runway, a wind of 7 knots, 250° from the heading direction carried the fire onto and around the rear fuselage. After the aircraft stopped, the hull was penetrated rapidly and smoke, possibly with some flame transients, entered the cabin through the aft right door which was opened earlier before the aircraft came to a halt. Subsequently fire developed within the cabin which destroyed the aircraft and took the lives of 55 persons onboard.

British Department of Transportation (DOT) concluded that the cause of the accident was an uncontained failure of the left engine, initiated by a failure of the No. 9 combustion can which had been the subject of a repair. A section of the combustion can, which was ejected forcibly from the engine, struck and fractured an underwing fuel tank access panel. The access panels have an impact strength that is 1/4 that of the lower wing skin, and therefore are more likely to fail. The resulting fire had catastrophic consequences primarily because of adverse orientation of the parked aircraft relative to the wind, even though the wind was light.

According to the British DOT, other major contributory factors were the vulnerability of the wing tank access panels to impact, a lack of any effective provision for fighting major fires inside the aircraft cabin, the vulnerability of the aircraft hull to external fire, and the extremely toxic nature of the emissions from the burning interior materials.

The forward section of the No. 9 combustion can was ejected through the left engine combustion casing, which was split open, causing substantial secondary damage to the engine and nacelle. A fuel tank access panel on the lower surface of the left wing immediately outboard of the engine had been punctured, producing a large hole in the base of the main fuel tank. The left engine nacelle and adjacent wing areas were damaged by fire and the wing suffered additional damage caused by an explosive overpressure within the fuel tank. The right wing and engine were undamaged.

The fuel was contained in three fuel tanks, all of which were integrally formed within the aircraft's wing structure. The two main tanks of 4,590 kg capacity each were enclosed (one in each wing) by the main torsion box, and extended from the root rib outboard to a position close to the wing tip; and a center auxiliary tank, which had a capacity of 7,416 kg.

Access to the interior of each main wing tank was provided by means of a total of 13 elliptically shaped removable access panels varying in size from approximately 18 by 10 in. inboard to 16 by

6 in. outboard, which were secured flush with the lower skin surface and sealed by an O-ring gasket. The access panels were manufactured from a cast aluminum alloy material and had stiffening webs integrally formed on the upper (internal) surface. The panels were nominally nonstressed components so far as flight loads on the wing were concerned; impact strength did not form a part of the design requirements for the wing lower skin, nor the access panel. The cast aluminum material had an impact strength approximately one-quarter that of the lower wing.

The center of a fuel tank access panel on the lower surface of the wing immediately outboard of the left engine was ruptured outwards, producing an 8- by 7-in. elliptic hole directly into the central region of the main fuel tank. The panel exhibited signs of having been struck forcibly on its lower (outer) surface.

The upper skin on the left wing was torn upwards, the corresponding sections of the lower skin were severely bulged downwards and the ribs inside the tank were buckled. According to the DOT, all of the damage to the left wing structure, with the exception of the broken access panel, was consistent with a rapid overpressure of the tank cavity resulting from the ignition of fuel vapor within the tank.

The combustion cans from the left engine of this aircraft and others from the same operator showed evidence of localized hot spots, i.e., areas of the can liner material exhibiting excessive overheat blistering and/or multiple cracking. The DOT states that such local effects can also be produced by different causes, such as a distorted fuel nozzle flow pattern, distortion of the dimensions of the can, or cooling airflow disturbance caused by repairs or faulty design/manufacture.

Since the temperature of the hot spot rose dramatically as peak power was approached, i.e., at a greater rate than simple theory would have predicted, the DOT hypothesized that a concentration of combustible reactants in the wall cooling layers became rich enough for combustion to begin next to the wall itself, elevating the liner temperature disproportionately.

According to the DOT, the explosive failure of the combustion chamber outer case (CCOC) and the damage to the adjoining tank access panel were clearly related events. Witness marks on the access panel fragments exactly matched the shape of the domed head of the separated No. 9 combustion can and the fan case fragment, and a smear of panel material was identified on the dome indicating beyond all doubt that it was this which struck and shattered the panel. It is evident that the dome was ejected through the disrupted engine casing as a result of the extremely rapid escape of high-pressure combustion air through the ruptured CCOC. The subsequent release of fuel from the damaged wing tank directly into combustion gases from the ruptured combustion chamber ignited and produced the catastrophic fire described above.

The wing tank access panel had an impact strength approximately one-quarter that of the lower wing skin. Neither the access panel nor the lower wing skin were designed to any impact resistance criteria, nor were they required to be.

A pool fire external to the aircraft resulted when fuel from the punctured wing came into contact with combustion gases escaping from the damaged engine. Although the dynamic fire plume

that ensued was visually very dramatic, the DOT determined that hull penetration was caused primarily by the quasi-static/static pooled fuel fire and the wind was the principal factor controlling the fire's behavior. The wind carried the external pooled fuel fire against and beneath the rear fuselage, giving rise to rapid fire penetration. Subsequently the wind induced an aerodynamic pressure field around the fuselage which drew combustion products into the hull, through the cabin interior, and out through open exits on the right side of the fuselage.

The Aircraft Accident Investigation Board (AAIB) concluded that a requirement should be introduced to ensure (1) existing external fuel tank access panels, which are vulnerable to impact from engine or wheel/tire failures on aircraft in service, are at least as impact resistant as the surrounding structure; and (2) the potential risk of damaging from debris impacts should be addressed in the future by appropriate design requirements covering debris ejection from engines and/or impact strength requirements for the airframe. The strength of the access panel has been increased to match that of the aircraft skin after this accident.

A.2.2 San Francisco, California, June 28, 1965.

According to the NTSB, the number three turbine disk in the No. 4 engine of a Boeing 707-321B failed due to a localized reduction in its cross-sectional area and overheated conditions due to rubbing between the turbine disk and the third stage turbine inner sealing ring immediately forward of the disk. The rubbing was the result of a transient loss of clearance between these parts on takeoff. The maximum difference in the thermal expansion rates between the rotating assembly and the outer turbine cases which support the inner sealing ring occurs 1-2 minutes after application of takeoff power.

The disk failure resulted in an explosion inside the No. 4 engine and its separation from the wing due to high vibration and out of balance oscillation of the rotating parts of the engine. The right outer wing was damaged so much in the lower load bearing skin and structure that the capability of the wing to sustain in-flight loads was reduced below the loads imposed and the outer wing panel separated from the wing. Fuel from the engine fuel line was then being pumped directly into the airstream. This fuel was ignited by an undetermined source shortly after the engine separated and resulted in an explosive separation of a portion of the lower wing skin.

An intermittent fire warning alerted the flight crew to the fire while they were going through the engine shutdown procedure following the failure of the No. 4 engine. The first officer then actuated the fire selector lever for the No. 4 engine and discharged both fire extinguisher bottles to the engine. The fire was observed to go out and did not recur. A fluid was observed streaming from the right wing for the duration of the flight. Fuel was still streaming from the right wing No. 4 tank after landing. The area around the fuel spill and the damaged wing area were foamed as a preventive measure while the passengers were deplaning.

The engine fuel line was pulled from the strut closure rib when the engine separated from the wing. Fuel was pumped through this line for an estimated 99 seconds at a rate of approximately 30,000 pounds per hour, until the fuel valve was shut off. A second fuel source was the fuel line on the forward face of the main spar which had a loosened fitting that leaked and supplied fuel

for a fire over the strut center spar between the front spar and the nacelle closure rib. A third possible fuel source was the ruptured slat hydraulic line in the inboard gap cover area.

According to the NTSB, the source of ignition could not be determined. The possible sources included the engine exhaust, hot turbine parts, or arcing from exposed electrical leads. The latter being the most probable source because there was an appreciable time lapse between observation of the fuel spray and ignition. Much of the upper wing surface was wetted by the fuel before ignition occurred.

Laboratory tests of fuel samples taken from the six remaining fuel tanks on the aircraft revealed no significant deviation from the specifications established for a Jet-A fuel. It was estimated by the NTSB that the fuel temperature in the tanks of N761PA at the time of the accident was between 70 and 80°F. This is below the static flammability limit, not taking into account variations to the flammability limits of fuel in a tank due to volume, size, shape, agitation, or other factors that affect a fuel tank ullage when the aircraft is in flight. (See section 3.)

Because the No. 4 main tank was full of fuel, it acted as a heat sink and probably prevented more extensive fire damage to that area of the upper wing surface. Based on the observed damage, the NTSB estimated that the fire in this area reached temperatures ranging from approximately 870-1165°F.

The right outboard wing panel top and bottom skin and ribs were damaged by an overpressure in the reserve tank. This is demonstrated particularly by the manner in which the lower skin separated from the aircraft, taking the attaching flanges of both spars with it. According to the NTSB, this is the result of a low-order¹ explosion and while the source of ignition could not be determined, it could have been autoignition, burnthrough, or hot-point ignition from a localized hot spot.

The explosion in the reserve tank was followed by the final separation of the wing and are not believed to have been simultaneous events. The NTSB believes that the indications of yaw and vertical oscillation on the flight recorder readout and the location of the wreckage on the ground indicate that the wing panel remained on the aircraft approximately 10-11 seconds after the separation of the lower skin panel.

A.2.3 San Francisco, California, September 18, 1970.

Approximately 16 seconds after takeoff, at an altitude of 525 feet m.s.l.², the No. 1 engine of a Boeing 747-121 sustained an uncontained failure of the second-stage turbine disk rim. The turbine blades and rim fragments penetrated the high-pressure turbine (HPT) case, engine cowling, and adjacent airplane structure. All fluid lines, electrical cables, and pneumatic ducts in the pylon area were severed causing an intense fire which extended over the top of the left wing and lasted approximately 3 minutes. Two fuel tank access plates on the bottom of the wing inboard of No. 1 pylon were also penetrated by turbine fragments.

¹ Used in this sense, low order indicates that the pressure wave moved at subsonic velocity.

² m.s.l. - Mean Sea Level.

The fire warning for the No. 1 engine came on simultaneously with the engine explosion. Emergency fire control procedures were initiated and executed. As a result of complete failure of the No. 1 hydraulic system, alternate extension of the body main landing gear, nose landing gear, and inboard trailing edge flaps was necessary for landing.

The National Transportation Safety Board determined that the probable cause of this incident was a progressive failure in the high-pressure turbine module in the No. 1 JT9D-3A engine. This failure was initiated by the undetected stress rupture fractures of several first-stage turbine blades and culminated in the inflight uncontained failure of the second-stage turbine disk rim.

Two holes were burned through the pylon outboard skin between nacelle stations 236 and 265 and nacelle water line 136 and 154. Much of the pylon outboard skin was discolored and buckled by heat. Although nacelle station 265.94 bulkhead remained otherwise intact, it also was discolored and buckled by heat.

Other fire and/or shrapnel damage included the left outboard flap, outboard aileron, No. 1 spoiler, flap track fairings, leading edge panels/fairings, wing leading edge support structure, and trailing edge panels.

The most severe damage was sustained by the underside of the left wing, both inboard and outboard of No. 1 pylon. The first and third fuel tank access plates outboard of the No. 1 pylon exhibited evidence of heat discoloration. Two fuel tank access plates between wing stations 950 and 1000 and between 975 and 1000 were punctured and were the source of profuse fuel leakage. These access panels have an impact strength that is 1/4 that of the lower wing skin, and therefore are more likely to fail. Although there was no ignition of the fuel which was leaking from these two access plates, the flames propagating over both the top and bottom of the wing posed a definite danger of ignition.

Gouges in the lower wing skin, inboard of No. 1 of the pylon, formed a pattern which ran diagonally inboard and rearward between wing stations 1070 and 940 and from the front spar to an area slightly aft of the fuel tank access plates. There were approximately 100 such gouges. Six relatively deep gouges were concentrated in an approximately 1-square-foot area at wing station 1035 just forward of the midspar. The deepest of these six gouges measured 0.187 inch in depth. Lower wing skin thickness at this point is 0.40 inch. Another concentration of gouges was located immediately forward of the fuel tank access plate between wing stations 975 and 1000. The deepest of these gouges measured 0.218 inch in depth. Lower wing skin thickness at this point is 0.326 inch.

According to the NTSB, the fire extinguishing agent discharged by the crew was ineffective in controlling or extinguishing the fire. The most serious impairment of the system's effectiveness occurred when the engine and pylon enclosures were penetrated during the turbine failure, allowing a substantial portion of the extinguishing agent to escape into the atmosphere. The fire inside of the pylon continued with such intensity that both of the agent containers became physically detached from their mountings and fell to the bottom of the pylon structure. This fact alone can leave little doubt that the fire continued for some time after the agent was discharged. The NTSB believes that the fire terminated only when the sources of flammable materials

became exhausted or in the case of the severed fuel line, when the firewall shutoff valve which was upstream from the break was closed by the flight crew.

The NTSB concluded that the fire which resulted from the turbine failure was terminated by the immediate response of the flight crew in successfully shutting off fuel supply to the No. 1 pylon. The fire extinguishing agent appeared to have little effect in combating the fire.

A.2.4 Jamaica, New York, November 12, 1975.

The No. 3 engine on a Douglas DC-10-30 disintegrated and separated after ingesting birds. Fire erupted on the right side of the aircraft. When the aircraft left the paved surface, integrity of the wing fuel tanks was lost and the structure of the aircraft was damaged.

Disintegration of the engine consisted of the separation of the compressor case and the fan assembly and the fracture of the fuel supply line in the leading edge of the pylon. Manufacturer's data show that, with the tank fuel pump on, the fuel flow through the 2-inch fuel line is between 150 and 160 gallons per minute. The NTSB calculated, based on the flight data recorder and the motion picture taken from the cockpit during takeoff and rollout, that 15 seconds elapsed from the 6,400-foot point on the runway to the point where the fuel shutoff was actuated. Therefore, about 40 gallons of fuel would have been expelled, and the aircraft would have traveled about 3,800 feet. After the fuel was shut off, sufficient fuel remained between the shutoff valve and the break in the fuel line to support combustion until the aircraft came to rest.

A.2.5 Sioux City, Iowa, July 19, 1985.

On July 19, 1989, a DC-10-10 had an uncontained engine failure resulting from the separation of the stage 1 fan disk from the No. 2 aft (tail-mounted) engine during cruise flight. The fragment ejected from the engine, which consisted of the stage 1 fan rotor assembly parts, penetrated the aircraft structure, and severed the hydraulic lines for the hydraulic systems No. 1 and No. 3 located in the right horizontal stabilizer. The No. 2 hydraulic systems are located next to the No. 2 engine accessory section and were damaged and separated by the force from the engine failure. The damage to all three hydraulic systems left the aircraft with no flight control.

The crew attempted to control and land the aircraft by using differential engine power from the two operating wing-mounted engines to control pitch and roll. Fuel was jettisoned to the level of automatic system shutoff, leaving 33,500 lbs. The airplane crashed during an attempted emergency landing, broke apart, and was consumed by fire. The NTSB concluded that the engine failure was caused by a near-radial, bore-to-rim fracture of the fan disk initiated from a fatigue region on the inside diameter of the bore. The fatigue crack occurred due to a previously undetected manufacturing defect.

Furthermore, the NTSB stated that the original design of the DC-10 should have considered the possible hydraulic system damage caused by random engine debris and should have better protected the critical hydraulic systems from a such effects. We understand that after this accident, redundant critical systems are now separated physically so as not to fail simultaneously

(i.e., to avoid a single point failure). Also, doubled-wall lines are used to minimize the leakage of flammable fluids.

A.3 PERTINENT ACCIDENTS INVOLVING MILITARY AIRCRAFT.

Due to some similarity between military cargo aircraft and large commercial aircraft, we expanded our search of uncontained engine failure accidents by contacting the Air Force Safety Agency. At our request, the Air Force queried their database for uncontained engine failures involving cargo planes from 1975 to date. We had no direct access to this database. We, however, identified 42 incidents for which we obtained short narratives. Seven of these incidents involve information potentially related to fuel release. Table A-1 summarizes these accidents.

TABLE A-1. SELECTED UNCONTAINED ENGINE FAILURES OF AIR
FORCE CARGO AIRCRAFT

	Year	Aircraft	Failure	Information Related to Potential Fuel Release
1	83	C-130E	1st stage turbine wheel	Mechanical damage to leading edge of wing, external tank, and pylon.
2	84	C-130E	2nd stage turbine	Mechanical damage in the wing nacelle firewall.
3	85	C-130E	Turbine spacer	Penetration of an external fuel tank containing 6,000 lb. of JP-4. There were no fire and no injuries.
4	85	C-5A	Turbine case penetration	Fire produced sheet metal damage to underside of wing, wing flap, and right side of fuselage.
5	87	C-5A	Compressor case penetration	Nitrogen discharged in the wing area, but no wing fire. Fuel release from the P&D valve upon landing.
6	87	KC-135A	Compressor case penetration	Smell of fire. About 100,000 lb. of fuel was jettisoned. Successful landing.
7	90	C-5A	Fan case penetration	Hole (2 to 3 inches in diameter) in the fuselage skin. The hydraulic return line was severed.

The reported accidents indicate significant mechanical damage (large holes) in the wing and fuselage of aircraft (cases 1, 2, and 7) and fire/thermal damage to the firewall (case 4) can occur. A greater potential for fuel release exists for fuel tanks that are integrated into these structures. However, several of the accidents reported that fuel was released, but there was no significant fire.

A.4 REFERENCES.

CAB Aircraft Accident Report, Pan American World Airways, Inc., B-707-321B, N761PA, San Francisco, California, June 28, 1965.

National Transportation Safety Board Aircraft Incident Report, American Airlines, Inc., Boeing 747-121, N743PA, San Francisco, California, September 18, 1970.

British Department of Transport Accident Report, Boeing 737-2367 Series 1, G-BGJL, Manchester International Airport, August 22, 1985.

National Transportation Safety Board Aircraft Accident Report, Overseas National Airways, Inc., Douglas DC-10-30, N1032F, John F. Kennedy International Airport, Jamaica, New York, November 12, 1975.

National Transportation Safety Board Aircraft Incident Report, United Airlines, McDonnell Douglas DC-10-10, Sioux City, Iowa, July 19, 1989.

APPENDIX B—ASPERITY FROM FRAGMENT IMPACT: ITS DETACHMENT AND HIGH TEMPERATURE FORMATION

Asperities on a fragment may reach high temperatures when the fragment hits the tank skin. There are two heating mechanisms as shown in figures B-1 and B-2.

Mechanism 1: The frictional force acting at the sides of the fragment may break asperities and then raise their temperature.

Mechanism 2: The compression force due to the impact acting at the front of the fragment may break asperities and then raise their temperature.

To estimate the asperity temperature, we assume that the work done to the asperity by either frictional force or compression force is completely converted to the thermal energy of the asperity. Thus

$$Ft = V\rho c\Delta T \quad (1)$$

where:

F: force acting on the asperity in its moving direction

t: thickness of the tank skin

a: size of the asperity, here for simplicity we assume the asperity shape is cubic with side length a

V: $= a^3$, volume of the asperity

ΔT : temperature increase of the asperity

A blade fragment has the following properties:

ρ : $= 4.85 \text{ g/cm}^3 = 302.6 \text{ lb/ft}^3 = 0.175 \text{ lb/in}^3$, density

c: $= 0.13 \text{ Btu/(lb)(F)}$, specific heat

Y: $= 190 \cdot 10^3 \text{ lbf/in}^2$, yield stress

From equation (1), we can obtain the temperature increase of the asperity as

$$\Delta T = \frac{F t}{V \rho c} \quad (2)$$

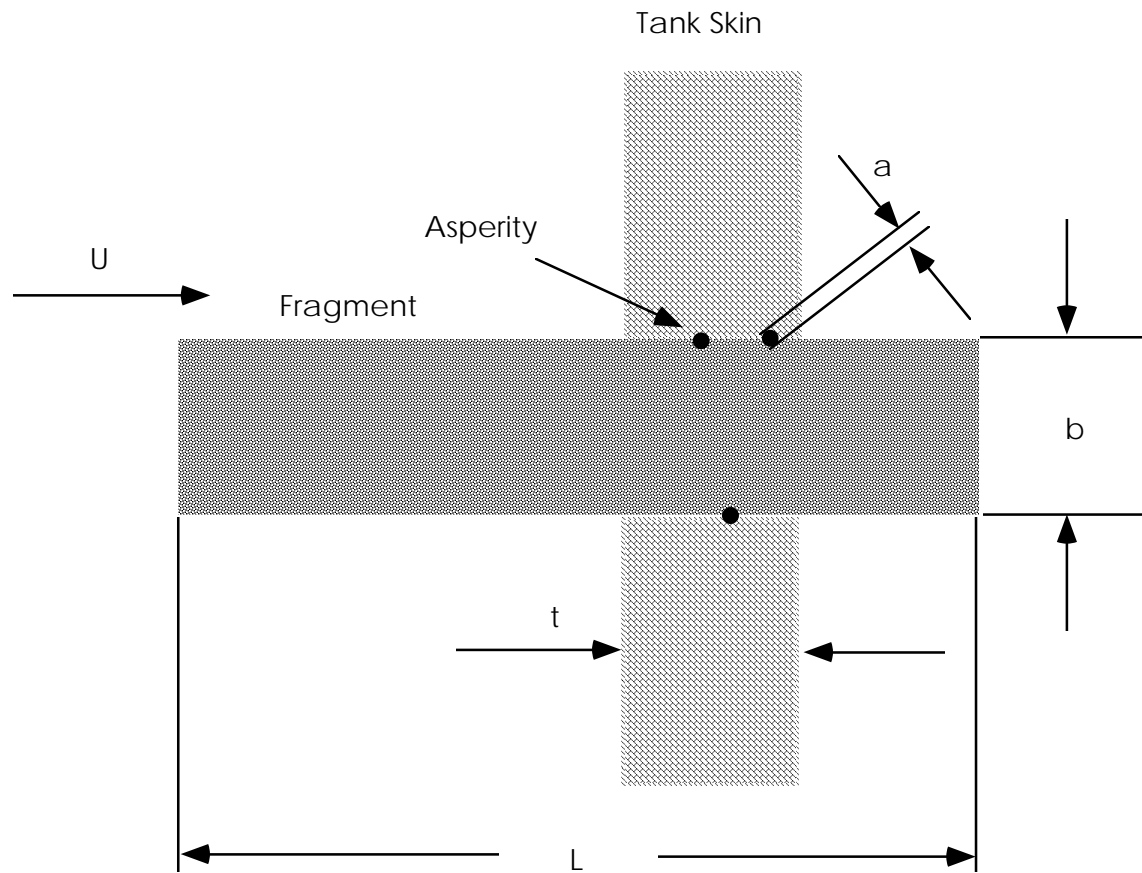


FIGURE B-1. SIDE FRICTION MECHANISM

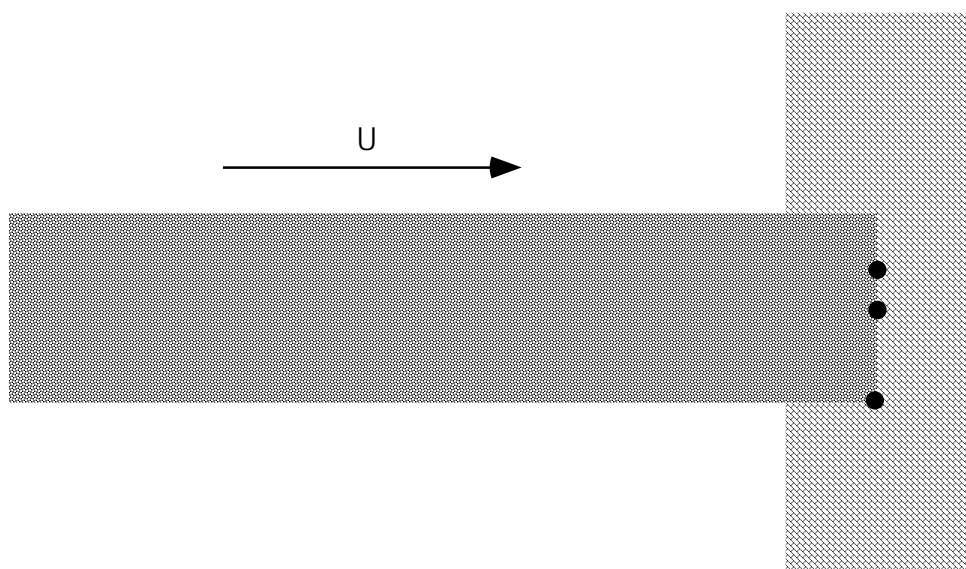


FIGURE B-2. FRONT COMPRESSION MECHANISM

The estimation of the temperature depends on the estimation of the force, F , acting on the asperity. We offer the following two simple approaches. Refinement of the estimation is subject to the availability of more data.

Method 1:

We assume that the force is equal to the yielding stress times the asperity side area, thus

$$\Delta T = \frac{Y a^2 t}{V \rho c} = \frac{Y t}{a \rho c} = \frac{190 \cdot 10^3 \frac{\text{lb}_f}{\text{in}^2} \cdot t}{a \cdot 0.175 \frac{\text{lb}_f}{\text{in}^3} \cdot 0.13 \frac{\text{Btu}}{\text{lb} \cdot ^\circ\text{F}} \cdot 1.8 \frac{^\circ\text{F}}{^\circ\text{C}} \cdot 778 \frac{\text{ft} \cdot \text{lb}_f}{\text{Btu}} \cdot 12 \frac{\text{in}}{\text{ft}}} = 497 \frac{t}{a} (^\circ\text{C}) \quad (3)$$

If $t/a = 10$, $\Delta T \approx 5000$ (C). This estimation of temperature increase may be overestimated due to (1) the negligence of heat loss to the tank skin and (2) the overestimation in force.

Method 2:

We assume that the work done on the blade by frictional force is equal to the kinetic energy loss of the blade, thus

$$F_b t = \frac{1}{2} M_b (U_1^2 - U_2^2) \quad (4)$$

where

- F_b : total frictional force acting on the blade
- M_b : mass of the blade fragment
- U_1 : velocity of the blade fragment before hitting the tank
- U_2 : velocity of the blade fragment after penetrating the tank skin

The force acting on the asperity can be obtained as

$$F = \frac{F_b a^2}{4bt} \quad (5)$$

Since F_b is acting on the whole blade, the $\frac{a^2}{4bt}$ factor provides the force acting on the asperity. $4bt$ is the approximate circumference area of the blade that contacts the tank skin.

The factor of 4 in equation 5 takes into account the whole contacting side of the blade. Assuming $U_2 = 0.9 U_1$ and $M_b = \rho b^2 L$, where b and L are the side and axial length scales of the blade fragment, respectively, see figure B-1, the temperature increase of the asperity is then

$$\Delta T \approx \frac{U_I^2 L b}{40 c t a} \quad (6)$$

Let $U_I = 500$ ft/s, $L = 4$ in, $b = 0.5$ in, $a = 0.01$ in, and $t = 0.1$ in, then

$$\Delta T \approx \frac{25 \cdot 10^4 \frac{ft^2}{s^2}}{40 \cdot 0.13 \frac{Btu}{lb \cdot F} \cdot 778 \frac{ft \cdot lbf}{Btu} \cdot 32 \frac{lb \cdot \frac{ft}{s^2}}{lbf} \cdot 1.8 \frac{F}{c}} \cdot \frac{4 in \cdot 0.5 in}{0.1 in \cdot 0.01 in} = 2146^\circ C \quad (7)$$

This estimation has assumed that velocity loss is 10 percent and the head-on hitting energy loss is negligible. More accurate estimation can be obtained upon receiving the fragment geometry, breaking hole size, and fragment's moving velocities before and after hitting the tank skin.

In summary, this appendix shows that hot spots can develop on fragments during impact and increase the probability of ignition. However, this effect was not included in section 4 because the initial temperature of the high-pressure turbine was already sufficiently high to produce ignition.